Supporting Information

Dynamic Covalent Bonds for Optical Data Storage: Harnessing $^1O_2$-Self-sensitization and Photoperoxidation for Information Encoding

*Ruben R. Ferreira, Daniel Wirtitsch, Jack Fletcher-Charles, Sofia Lopez, Cristina E. Hoppe, Michael Trupke, Laura Maggini, and Davide Bonifazi**

R. R. Ferreira, L. Maggini, D. Bonifazi
Institute of Organic Chemistry, University of Vienna. Währinger Strasse 38, A-1090 Vienna, Austria
E-mail: davide.bonifazi@univie.ac.at

D. Wirtitsch, M. Trupke
Institute for Quantum Optics and Quantum Information (IQOQI) Vienna, Austrian Academy of Sciences, Boltzmanngasse 3, A-1090 Vien-na, Austria

J. Fletcher-Charles
School of Chemistry, Cardiff University, Park Place Main Building, Cardiff CF10 3AT, United Kingdom

S. Lopez, C. Hoppe
División Polímeros Nanoestructurados, Instituto de Investigaciones en Ciencia y Tecnología de Materiales (INTEMA), UN-MdP−CONICET y Departamento de Química, UNMdP, Av. Cristóbal Colón 10850, B7606BWV Mar del Plata, Buenos Aires, Argentina

Table of contents

1. General remarks

1.1 Instrumentation

Thin layer chromatography (TLC) was conducted on pre-coated aluminum sheets with 0.20 mm Merck Millipore Silica gel 60 with fluorescent indicator F254. TLC plates were visualized by exposure to ultraviolet light (254 or 366 nm).

Column chromatography was carried out using Merck Gerduran silica gel 60 (particle size 40-63 μm).

Melting points (mp) were measured on a Leica Galen III microscope equipped with a heating block and a Hg thermometer (T_{max} = 350 °C) on a microscope slide under air, and are uncorrected.

Nuclear magnetic resonance (NMR) characterizations were performed at the NMR center of the University of Vienna. NMR spectra were recorded on Bruker spectrometer AV III HD 700, AV III 600 or AV NEO 400. ^{1}H NMR spectra were obtained at 700 or 400 MHz, ^{13}C NMR spectra at 176 MHz. All spectra were obtained at room temperature. Carbon spectra were acquired with a complete decoupling for the proton. Proton and carbon chemical shifts are reported in parts per million (ppm, δ scale) according to tetramethylsilane ($\delta_H = \delta_C = 0$ ppm) using the solvent residual signal as an internal reference ($CDCl_3$: $\delta_H = 7.26$ ppm, $\delta_C = 77.16$ ppm; DMSO-d_6: $\delta_H = 2.50$ ppm). Coupling constants (*J*) are given in Hz. Resonance multiplicity is described as s (singlet), d (doublet), t (triplet), m (multiplet), and br (broad signal).

Infrared spectra (IR) were recorded on a Bruker Alpha FT-IR spectrometer in ATR mode. Selected absorption bands are reported in wavenumbers (cm^{-1}).

High-resolution mass spectrometry (HRMS) analyses were performed at the Mass Spectrometry Centre of the University of Vienna. ESI mass spectra were obtained on a Bruker maXis UHR ESI-Qq-TOF mass spectrometer in the positive ion mode, LD and MALDI mass spectra on a Bruker Autoflex Speed LD-timsTOF or MALDI-timsTOF (matrix: 2-[(2E)-3-(4-tert-butylphenyl)-2-methylprop-2-enylidene]malononitrile (DCTB)) mass spectrometer.

Ultraviolet-visible absorption spectroscopy was recorded on a Cary 5000 (Agilent Technologies, US) UV-Vis-NIR Spectrophotometer running in double beam mode with a matched pair of quartz absorbance cuvettes (1 x 1 cm). All absorption measurements were performed at 21 °C unless specified otherwise. The absorbance of oxygen-free solutions was measured using a custom-built quartz cuvette. The molar attenuation coefficient (ε) was

determined by dissolving a known amount of compound and diluting the resulting stock solution to achieve 5 solutions with an appropriate concentration for measurements (absorbance < 0.5). The plot of absorbance versus concentration was fitted with a linear function and the molar attenuation coefficient obtained from the slope.

Ultraviolet-Visible emission spectroscopy. The photoluminescence (PL) excitation and emission spectra, absolute quantum yield, and decay curves were recorded on a FLS1000 photoluminescence spectrometer (Edinburgh Instruments, UK). The spectrometer was equipped with excitation and emission double grating Czerny-Turner monochromators, a photomultiplier detector with extended near-infrared sensitivity (PMT-980), fitted with a gating circuit and thermoelectrically cooled to -20 °C with a fan-assisted Peltier element, and a High Speed PMT detector with a response width < 180 ps operating at 0 °C. All samples were prepared in air-equilibrated extra dry 99+% 2-methyltetrahydrofuran (Thermo Fisher, stabilizer free). The maximum absorbance of all solutions was adjusted to < 0.1 to avoid inner filter effect. For oxygen-free measurements, the solutions where degassed by performing multiple cycles of freeze-pump-thaw (typically 5), and the headspace was filled with nitrogen (≥ 99.999%). Low temperature (77 K) measurements were carried out using an Optistat DN liquid nitrogen cryostat (Oxford Instruments, UK) fitted in the FLS1000 spectrometer sample chamber. The samples were placed in a custom-built cryogenic 1x1 cm quartz cuvette and held in a static nitrogen atmosphere. Glassy matrix was achieved by slowly lowering the temperature (20 °C/min). For steady-state measurements, the samples were excited using a 450 W ozone-free continuous Xenon arc lamp. Time-resolved measurements in the ns range were performed by irradiating the samples with a nano-pulsed laser (EPL-405) and acquired using the High Speed PMT detector in Time-Correlated Single Photon Counting (TCSPC) mode. The tail portion of the decay curves were fitted using the FAST software (Edinburgh Instruments, UK), following a single exponential model with y-offset (background-offset):

$$I(t) = A + B \cdot e^{\frac{-t}{\tau}} \quad (1)$$

where A is the y-offset, B the pre-exponential factor, and τ the lifetime. For decays close to the pulse width of the light source, the instrument response function (IRF) was measured using a Ludox® solution (at room temperature) or using the sample itself (at low temperature). In both cases the count rate was adjusted using a computer-controlled neutral density filter wheel in order to match the count rate of the sample emission. In these cases, the decay lifetime was obtained by performing a reconvolution fit using the FAST software. Absolute quantum yields were measured using an integrating sphere (internal diameter 120 mm) fitted on the FLS1000

sample chamber. The samples and blank reference (solvent) were placed in a 1 x 1 cm fluorescence quartz cuvette and the calculations were done using the "direct excitation" method following the equation:

$$\Phi = \frac{E_B - E_A}{S_A - S_B} \quad (2)$$

where E_B and E_A correspond to the integrated fluorescence emission of the sample and blank reference (solvent), respectively. S_A and S_B refer to the integrated excitation scatter region of the reference and the sample, respectively. For measuring the scatter region, and avoid detector saturation, a neutral density filter (OD = 2) was placed between the integrating sphere exit and the detector to attenuate the signal. A fixed excitation bandwidth of 3 nm was used to ensure the determination of the sample absorption with high accuracy (step = 0.1 nm), while the emission bandwidth was chosen to obtain a strong sample emission signal (peak emission > 10^4 cps). The optical bandgap E_g^{00}, was calculated using the intercept of the excitation and emission spectra (λ_{00}) following equation:

$$E_g^{00}(\text{eV}) = 1240/\lambda_{00} \quad (3)$$

Electrochemical analysis. Cyclic voltammetry experiments were performed at room temperature in CH_2Cl_2 purified by a SPS system (MBraun, DE), using an Autolab PGSTAT204 potentiostat (Metrohm, DE). A conventional three-electrode electrochemical cell connected to an argon source and an oil bubbler was used. Dry argon gas was bubbled through the sample solution for at least 15 min prior to each measurement and the headspace was continuously flushed throughout the experiment. A pre-bubbler filled with solvent was used in order to prevent evaporation. Platinum disk (3 mm diameter) was used as a working electrode, Pt wire as auxiliary electrode, and an Ag/AgCl electrode as reference.

The platinum working electrode was polished on a pad using alumina slurry and washed with deionized water before each experiment; the Pt wire was flame-cleaned. Tetrabutylammonium hexafluorophosphate (Alfa Aesar, $TBAPF_6$) was twice recrystallized from absolute ethanol prior to use and it was added to the solution as a supporting electrolyte at a concentration of 0.1 M. Decamethylferocene (Sigma Aldrich) was used as an internal reference. The formal redox potentials (half-wave potentials) were calculated using the formula:

$$E_{1/2} = \frac{E_{pa} + E_{pc}}{2} \quad (4)$$

where E_{pa} is the peak anodic potential and E_{pc} is the peak cathodic potential. The energy of the HOMO was estimated using the following equation:

$$E_{HOMO}(\text{eV}) = -\left(E_{1/2}^{ox}\right) - 4.8 \quad (5)$$

where E_{ox} is the half-wave oxidation potential (vs Fc/Fc^+) and 4.8 is the HOMO energy of ferrocene in vacuum. To reference the oxidation potentials vs Fc/Fc^+, we experimentally determined the potential of the $DmFc/DmFc^+$ redox couple to be -0.54 V vs Fc/Fc^+.

Spectroelectrochemical characterization was performed using a thin layer quartz cuvette (path length of 1 mm) equipped with an optically transparent platinum minigrid working electrode, platinum wire auxiliary electrode, and an Ag/AgCl reference electrode.

X-ray measurements were performed at the Centre for X-ray Structure Analysis of the University of Vienna. X-ray intensity data were measured at 100 K on a STOE Stadivari diffractometer equipped with dual radiation source Mo and Cu Kα, and a Dectris EIGER2 R 500K detector. The structures were solved ab initio and refined by full-matrix least-squares techniques. Hydrogen atoms were inserted at calculated positions using AFIX instructions, while all other atoms were refined with anisotropic displacement parameters. The following softwares were used: STOE software package for collecting crystal data and image processing, STOE LANA for scaling and absorption correction,[1] SHELXT-2018/2 for structure solution,[2] SHELXL-2018/3 for structure refinement,[3] SHELXLE version 1378 and OLEX2-1.5 as graphical user interfaces.[4-5] Crystal data, data collection parameters and structure refinement details are given in Tables S1–S2. Structures have been deposited in the Cambridge Structural Database (CSD) with the following deposition numbers: 2275542 (**4**), 2283987 (**4-EPO**). These data are provided free of charge by the joint Cambridge Crystallographic Data Centre and Fachinformationszentrum Karlsruhe Access Structures service via www.ccdc.cam.ac.uk/structures.

Optical microscope images were acquired using a DM2500 (Leica, DE) optical microscope equipped with an HC PL FLUOTAR 10x/0.32 objective and a Flexacam c1 12MP camera.

Spin coating was done in a H6-23 spin coater (Laurell, US) using the following program: 1200 rpm for 30 s, 1500 rpm for 20 s, 1800 rpm for 10 s.

1.2 Materials and Methods

Chemicals were purchased from Sigma Aldrich, Acros Organics, TCI, Alfa Aesar, Fluorochem, Thermo Fisher Scientific and BLDpharm and used without further purification. Anhydrous toluene, diethyl ether, and tetrahydrofuran (THF) were dried on a MBraun SPS-800 solvent purification system. Deuterated solvents were purchased from Eurisotop. Anhydrous conditions were achieved by drying glassware in an oven at 120 °C for at least 4 h, followed by purging with argon. The inert atmosphere was maintained using argon-filled balloons equipped with a syringe and needle that was used to pierce the silicon septa used to close the flask's necks. The addition of liquid reagents was performed using argon-purged plastic syringes. -78 °C baths were prepared using acetone/dry ice.

2. Equipment

2.1 Irradiation Lamp

Initial irradiation studies in solution were performed on a modified commercial setup (Figure S1) consisting of a lamp housing equipped with a 1000 W Xenon arc light source (Ushio, JP) and a rear reflector (Quantum Design, DE), a Czerny-Turner computer-controlled monochromator (MSH-300, Quantum Design, DE) with a focal length of 300 mm, 2 condenser optics, an electronic shutter with an external timing circuit (Quantum Design, DE), and a custom-built 3D printed sample holder. The manual slits located at the monochromator entrance and exit were used in their fully opened position (10x20 mm).

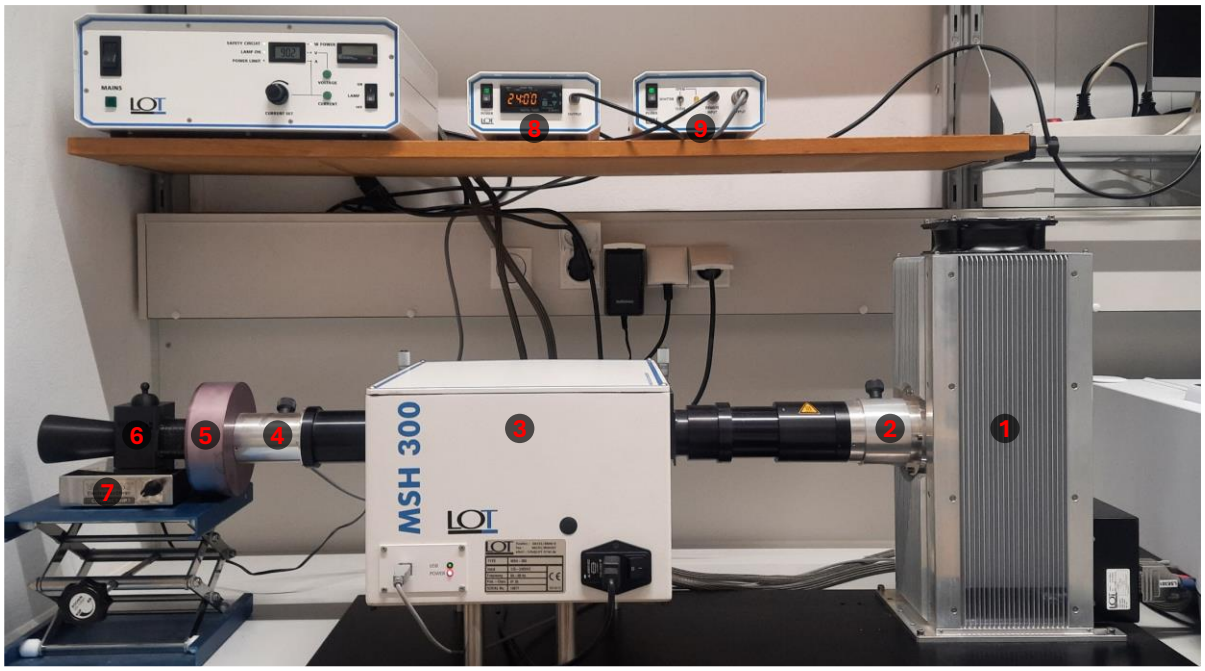

Figure S1. Picture of the irradiation lamp setup used for irradiation of solutions: 1 – Lamp housing; 2 – f/4 condenser optic; 3 – monochromator; 4 – f/4 condenser optic; 5 – electronic shutter; 6 – sample holder; 7 – magnetic stirrer; 8 – timer; 9 – electronic shutter controller.

2.2 High-power LED

For high-power irradiation in solution and photochromic patterning of thin-films, we used a custom-built setup consisting of a high-power green LED soldered to a metal core PCB (LZ4-00G108, Led Engin, US), attached to an aluminum heatsink (SA-LED-151E, Ohmite, US) using thermal compound (MX-4, ARCTIC GmbH, DE). The LED was powered using a laboratory power supply (BT-153, Conrad Electronic, DE) running in constant current mode. The irradiation time was controlled using a custom-built timer (Figure S2a) comprising of an Arduino uno rev 3 (Arduino, IT) with an LCD keypad shield (HD44780, AZ-Delivery Vertriebs GmbH, DE) and a 5 V relay (KY-019, AZ-Delivery Vertriebs GmbH, DE). For macro photowriting of thin films, the LED assembly was attached to a custom-built 3D printed holder fitted with an appropriate 3D printed black mask (Figure S2 b). For kinetic measurements, thin films were attached to the solid film holder of the Cary 5000, fitted with a custom-built 3D printed holder, allowing the LED assembly to be fitted and removed without moving the film (Figure S2 c-d).

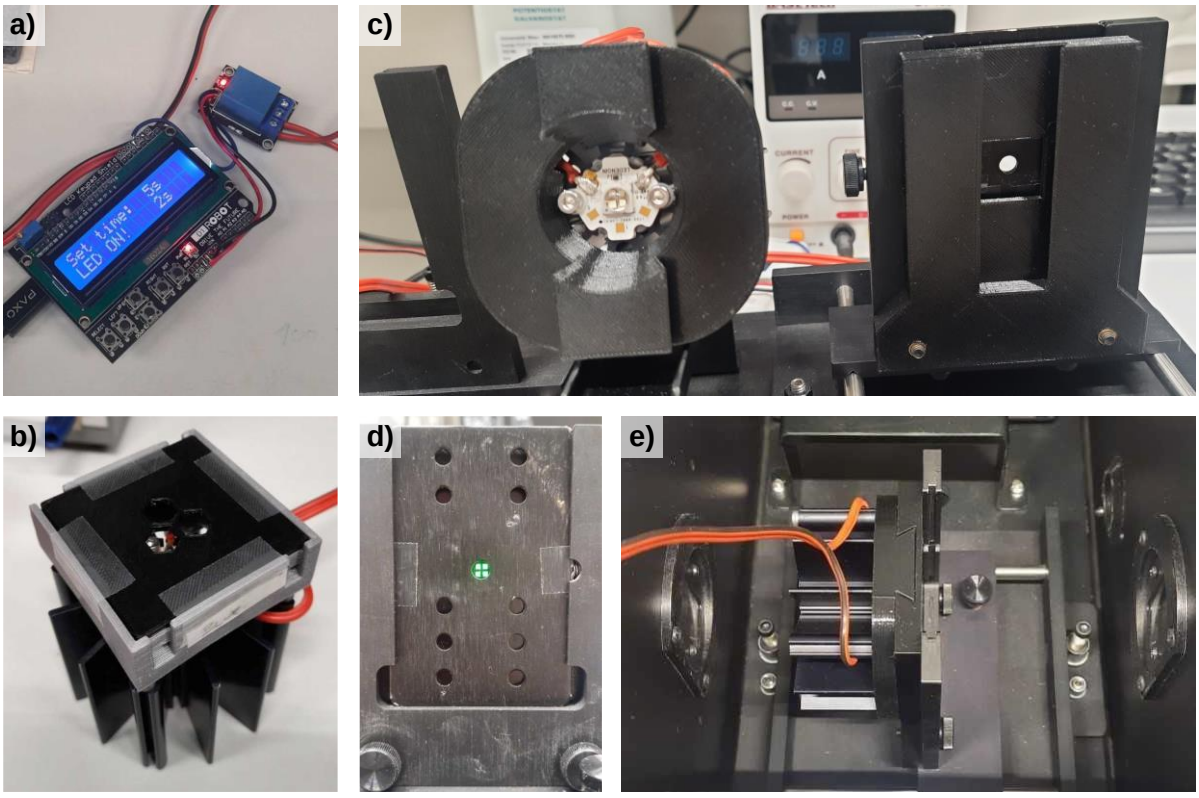

Figure S2. Pictures of the experimental setups used for irradiation of thin films using the high-power green LED.

2.3 Photodiode

The irradiation power was controlled by measuring the power output of the LED using a photodiode (FDS100-CAL, Thorlabs, US) and adjusting the current in the LED power supply. The photodiode was assembled following the recommended circuit by Thorlabs (Figure S3a). Briefly, the photodiode cathode was connected to a noise filter consisting of a 1 kΩ resistor connected in parallel with a 0.1 µF capacitor. A bias voltage (20 V) was applied between the noise filter and the circuit ground, and a load resistor (50 Ω) was placed between the photodiode anode and the circuit ground.

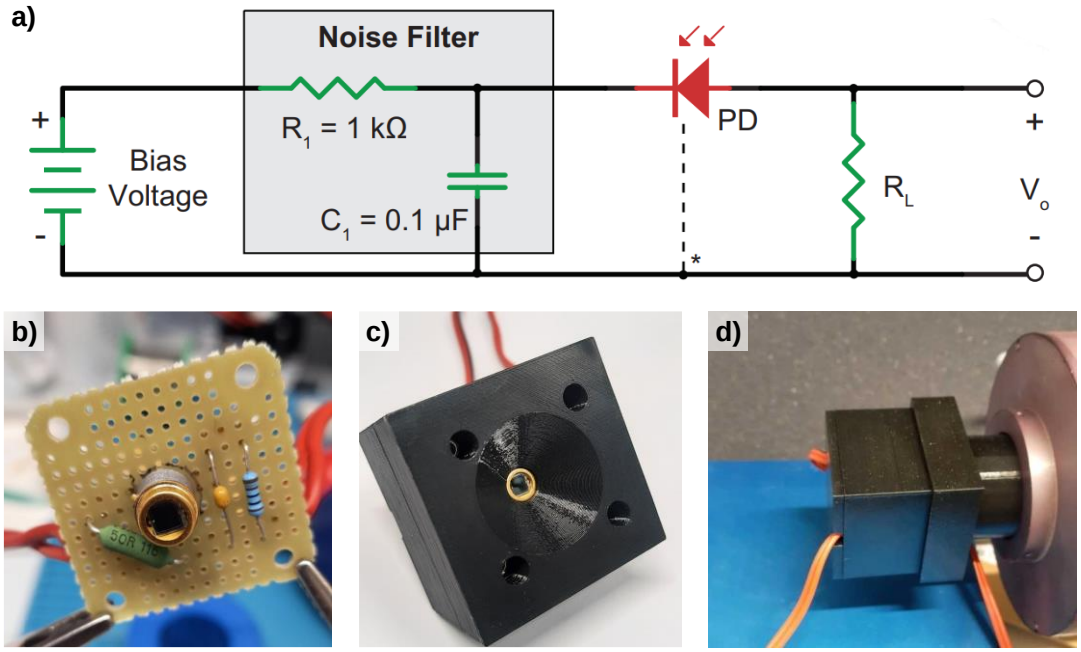

Figure S3. Photodiode electric circuit and setup.

The potential drop across the photodiode anode and the circuit ground was measured using a multimeter (EX330, Extech Instruments, US) and the irradiance power was calculated using the following equation:

$$P = \frac{V_0}{R \times R_L}$$

Where P is the irradiance power, V_0 is the measured potential drop, R is the responsivity at the selected wavelength (taken from the photodiode calibration sheet), and R_L is the load resistance (50 Ω). The photodiode responsivity was extracted from the calibration certificate provided by Thorlabs.

2.4 Laser

The laser writing and readout was done in a home-built confocal microscope setup, typically encountered in experiments using nitrogen vacancy centers in diamond. We employed a 520 nm, 80 mW laser diode (Roithner LD-520-80MG) which was coupled into a polarization maintaining single mode optical fiber to clean up the beam profile resulting in a gaussian beam shape. The rise time of the laser diode was measured to be 20 ns. The diode was driven by a directly TTL switchable diode driver designed for spike-free switching (IC Haus HG1D), analog modulated by an arbitrary waveform generator (Siglent SDG2042x). After the fiber, we opted for a maximum laser power of 4 mW to not extraneously drive the laser diode. The beam is focused on the sample by using an air objective (Nikon N60X-PF) with a numerical aperture of 0.85. During illumination, any backscattered laser light is filtered out from the collected light by using a 650 nm long-pass filter. The luminescence is collected with an optical fiber (Thorlabs P5-SMF28) that acts as a pinhole and detected by an avalanche photodiode. TTL pulses for fast switching and timing are provided via a home-built pulse generator with 1 ns time resolution based on the Red Pitaya STEMlab125.10. The samples were mounted on a Thorlabs MAX383 3-axis piezo stage with included stepper motors for positioning of the laser written optical data spots and to perform scans of the written regions.

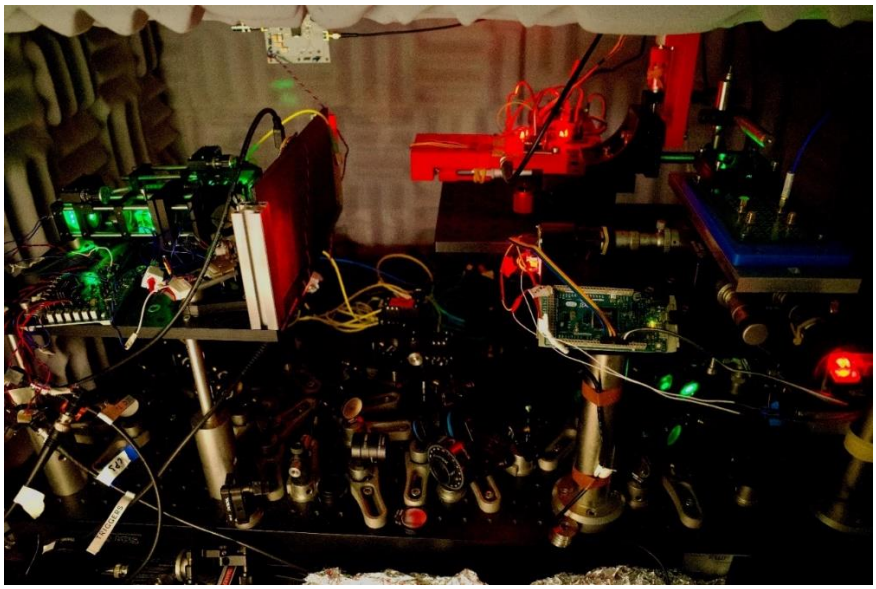

Figure S4. Laser setup. Left: 520 nm excitation source coupled into a single mode polarization maintaining fiber. Middle: Fluorescence collection optics including optical filters and collimation optics. Right: Piezo stage for positioning, PCB mount for samples and objective for laser writing.

2.5 Spray coater

Spray coating of thin films was performed on a modified Original Prusa i3 MK3S+ 3D printer (Prusa Research, CZ). The original 3D print head was replaced with a 3D printed PLA holder for a hand-held Fengda FE-134K professional airbrush (Ningbo Bida Machinery Manufacture Co., Ltd, CN). The airbrush was supplied with 0.7 bar of nitrogen. During the spray coating process, the gun was held vertical and parallel to the substrate, at a fixed distance of 6 cm. The X and Y axis were programmed to move in order to create alternating horizontal and vertical patterns with ≈50% overlap. The 3D printer heat bed was used to heat the substrate to 50 °C to facilitate solvent evaporation during spray coating and to fully dry the substrate afterwards.

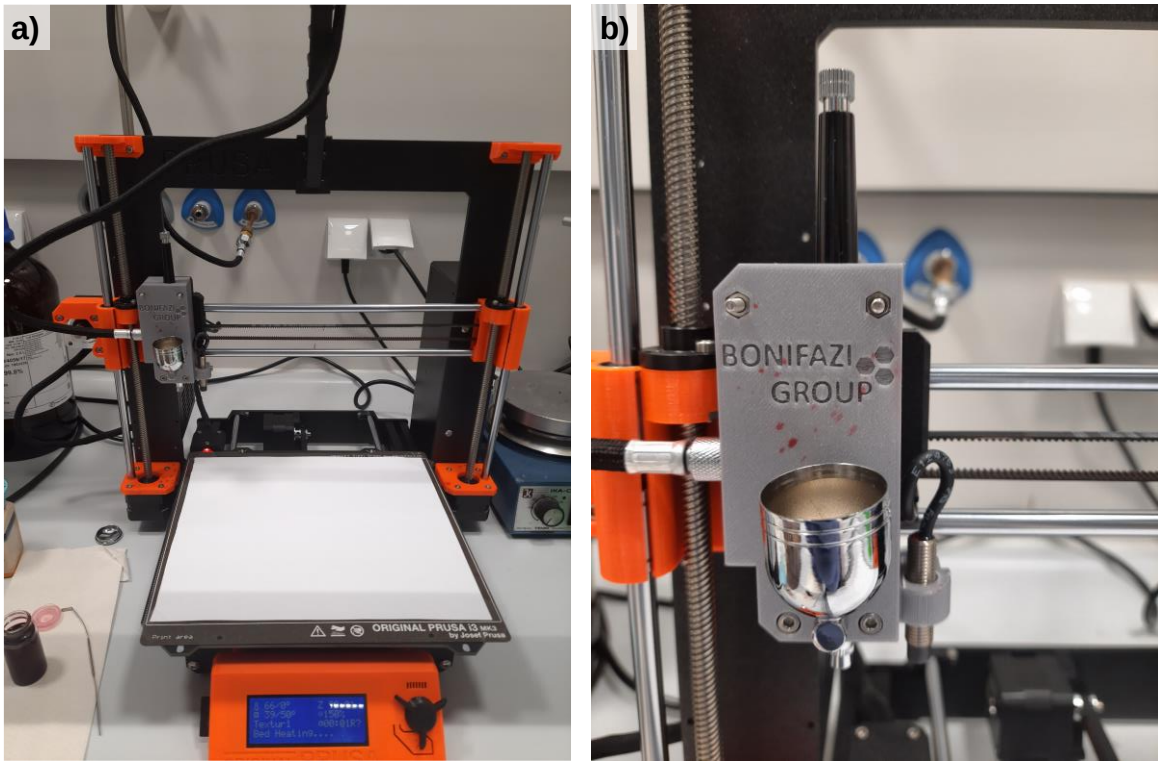

Figure S5. Spray coating setup: a) modified 3D printer; b) 3D printed airbrush holder.

3. Synthetic procedures

1,5-dichloro-9,10-bis(2-methoxy-4-methylphenyl)-9,10-dihydroanthracene-9,10-diol (1)

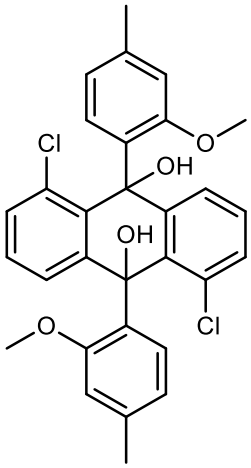

2-Bromo-5-methylanisole (808 mg, 4.02 mmol) was weighed into a 100 mL oven-dried round-bottom flask. The system was then put under an argon atmosphere, flushed for 10 min, and dry THF (20 mL) was added. The flask was cooled to -78 °C and *n*-BuLi (1.61 mL, 4.02 mmol) was added, after which the reaction was stirred at - 78 °C for 1 h. Meanwhile, a suspension of 1,5-dichloroanthraquinone (371 mg, 1.34 mmol) in THF (10 mL) was stirred at rt for 1 h after which was added to the starting material at -78 °C. The cooling bath was removed, and the reaction was stirred at rt for 24 h. The reaction was quenched by drop-wise addition of water (20 mL), the organic phase was separated and extracted with CH_2Cl_2 (3 x 40 ml). The combined organic layers were dried over $MgSO_4$, filtered, and concentrated *in vacuo*. The desired product was purified by trituration with MeOH and collected by filtration. Product isolated as a mixture of atropisomers (white powder, 590 mg, 84 % yield). **Mp** 225 – 228 °C. **^{1}H NMR** (700 MHz, $CDCl_3$) δ (ppm): 8.02 (br, 2H), 7.40 (d, *J* = 7.7 Hz, 2H), 7.11 – 7.06 (m, 4H), 6.91 (d, *J* = 7.2 Hz, 2H), 6.53 (s, 2H), 3.24 (s, 6H), 2.32 (s, 6H). **^{13}C NMR** (176 MHz, $CDCl_3$) δ (ppm): 155.1, 143.3, 138.7, 135.5, 133.1, 131.4, 130.2, 128.2, 128.0, 121.3, 114.5, 56.1, 21.5. **HRMS** (MALDI/tims-TOF): *m/z* calcd for $[C_{30}H_{26}Cl_2O_4Na]^+$: 543.1100 $[M+Na]^+$; found: 543.1100. **FTIR** (ATR) ν (cm^{-1}): 3561, 3407, 3061, 2922, 2853, 1610, 1578, 1501, 1455, 1429, 1406, 1282, 1255, 1191, 1162, 1140, 1120, 1036, 971, 933, 901, 816, 794, 761, 743, 702, 593, 549, 476, 416.

1,5-dichloro-9,10-bis(2-methoxy-4-methylphenyl)anthracene (2)

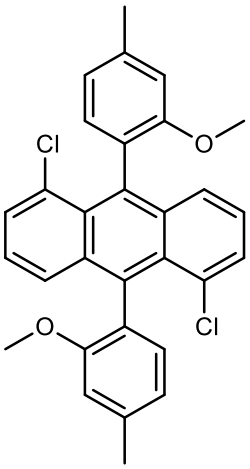

1 (583 mg, 1.12 mmol) was weighed into a round bottom flask, THF (10 mL) was added, followed by the addition of a solution of $SnCl_2$ (2 g) in concentrated HCl (2 ml). The reaction was stirred at rt for 2 h after which it was diluted with water (20 mL). The white precipitate formed was filtered off and washed with water and 1 M HCl. This gave the desired product as a mixture of atropisomers (pale-yellow powder, 468 mg, 86 % yield). **Mp** 261 – 264 °C. **^{1}H NMR** (700 MHz, $CDCl_3$) δ (ppm): 7.61 – 7.59 (m, 2H), 7.46 – 7.45 (m, 2H), 7.14 – 7.11 (m, 2H), 7.05 – 7.04 (m, 2H), 6.93 – 6.86 (m, 4H), 3.72 – 3.68 (m, 6H), 2.53 (s, 6H). **^{13}C NMR** (176 MHz, $CDCl_3$) δ (ppm): 158.1, 139.4, 134.1, 134.0, 133.8, 133.8, 132.4, 132.0, 131.4, 131.4, 129.2, 127.5, 127.4, 127.3, 127.1, 124.3, 124.3, 121.0, 120.9, 111.6, 55.7, 55.6, 21.9. **HRMS** (MALDI/tims-TOF): *m/z* calcd for $[C_{30}H_{24}Cl_2O_2]^+$: 486.1148 $[M]^+$; found: 486.1141. **FTIR** (ATR) ν (cm^{-1}): 2952, 2830, 1609, 1571, 1509, 1458, 1406, 1335, 1281, 1257, 1169, 1139, 1113, 1083, 1036, 982, 925, 900, 846, 795, 728, 682.

6,6'-(1,5-dichloroanthracene-9,10-diyl)bis(3-methylphenol) (3)

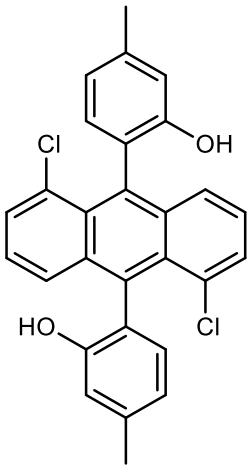

2 (100 mg, 0.205 mmol) was weighed into a 25 mL oven-dried round-bottom flask. The system was then put under an argon atmosphere, flushed for 10 min, and dry CH_2Cl_2 (10 mL) was added. The flask was cooled to -78 °C and BBr_3 (0.615 mmol in hexane) was added. The reaction was allowed to warm up to rt and stirred overnight (16 h) in the dark. The reaction was quenched with dropwise addition of a 6% ammonia solution (5 mL). The crude was extracted using CH_2Cl_2 (3 x 35 ml). The organic layers were combined and washed with brine (80 mL), dried over Na_2SO_4, filtered, and concentrated under reduced pressure. This gave the desired product as a mixture of atropisomers (dark yellow powder, 101 mg, quant. yield). **Mp** 235 – 238 °C. **^{1}H NMR** (700 MHz, CD_2Cl_2) δ (ppm): 7.70 – 7.68 (m, 2H), 7.5 – 7.56 (m, 2H), 7.27 – 7.25 (m, 2H), 7.03 – 6.87 (m, 6H), 4.58 (br, 2H), 2.48 (s, 6H). **^{13}C NMR** (176 MHz, CD_2Cl_2) δ (ppm): 154.2, 140.8, 134.8, 132.8, 132.4, 132.1, 131.7, 131.6, 130.7, 130.6, 128.5, 128.4, 127.5, 127.2, 126.1, 126.0, 124.5, 124.3, 121.9, 121.8, 116.3, 116.2, 21.6. **HRMS** (MALDI/tims-TOF): *m/z* calcd for $[C_{28}H_{20}Cl_2O_2]^+$: 458.0835 $[M]^+$; found: 458.0839. **FTIR** (ATR) ν (cm^{-1}): 3367, 2921, 1615, 1576, 1518, 1441, 1411, 1287, 1205, 1174, 1101, 985, 942, 858, 806, 784, 730, 699, 682, 606, 584, 553, 492, 464, 423.

2,10-dimethylbenzo[1,2,3-kl:4,5,6-k'l']dixanthene (4)

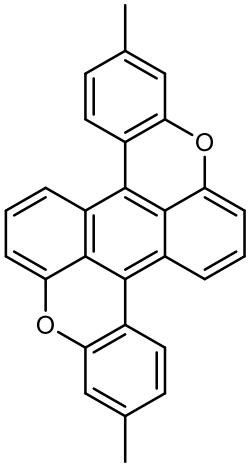

3 (303 mg, 0.66 mmol) and K_2CO_3 (303 mg, 2.19 mmol) were weighed into a round bottom flask. The flask was flushed with nitrogen, DMSO (80 mL) added, and the reaction heated to 140 °C for 2 h. The mixture was cooled, diluted with water, extracted with DCM (2 x 50 ml), dried over $MgSO_4$, and concentrated in vacuo. Purification by filtration with alumina afforded the product (dark red powder, 170 mg, 67% yield). **Mp** 291 – 293 °C. **^{1}H NMR** (400 MHz, DMSO) δ (ppm): 8.10 (d, *J* = 4.0 Hz, 2H), 8.08 (d, *J* = 3.3 Hz, 2H), 7.46 (t, *J* = 8.2 Hz, 2H), 7.14 (s, 2H), 7.09 (d, *J* = 8.3 Hz, 2H), 7.04 (d, *J* = 7.5 Hz, 2H), 2.39 (s, 6H). **HRMS** (LD/tims-TOF): *m/z* calcd for $[C_{28}H_{18}O_2]^+$: 386.1301 $[M]^+$; found: 386.1299. **FTIR** (ATR) ν (cm^{-1}): 2912, 1603, 1451, 1422, 1405, 1306, 1268, 1243, 1211, 1131, 1083, 1061, 813, 776, 715. Crystal suitable for X-ray diffraction was obtained by slow evaporation of $CDCl_3$ (CCDC #2275542 – see Table S1).

4. NMR spectra

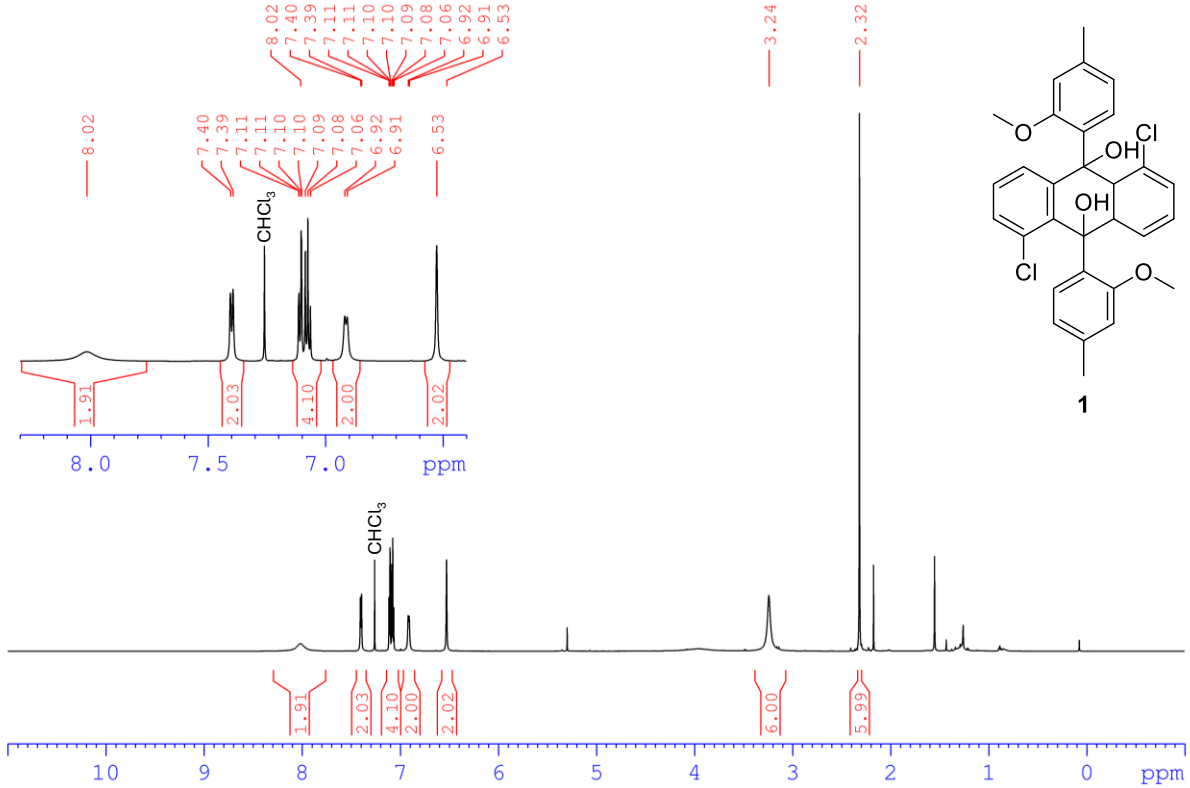

Figure S6. ^{1}H NMR (700 MHz, $CDCl_3$) spectrum of **1**.

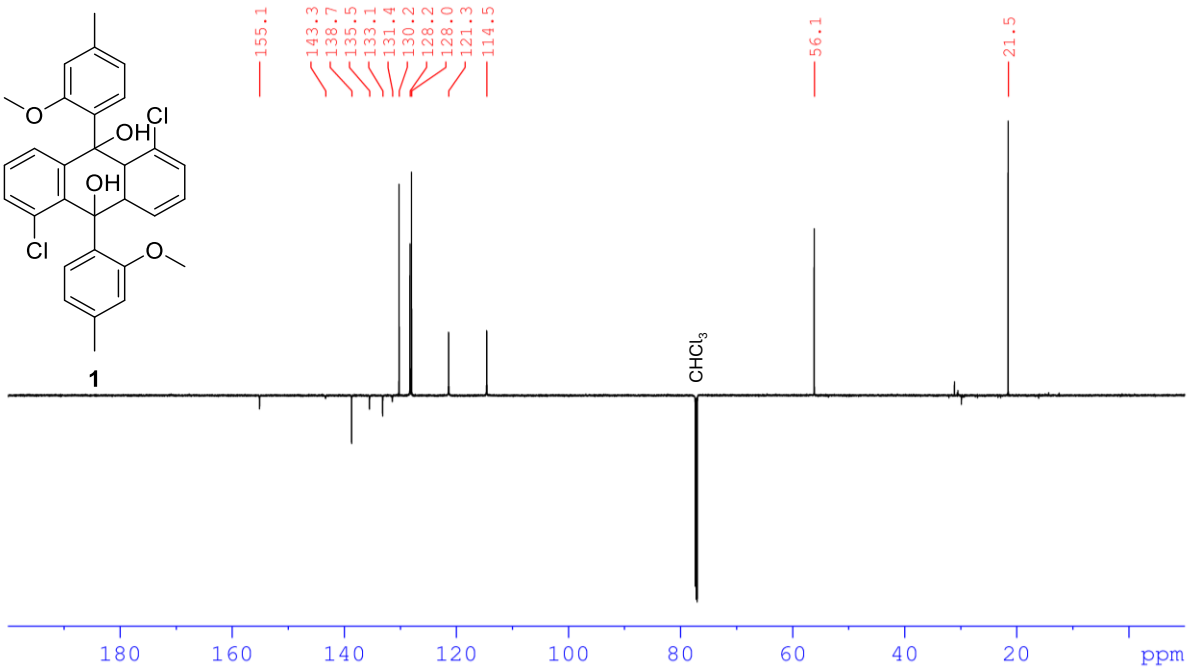

Figure S7. ^{13}C NMR (176 MHz, $CDCl_3$) spectrum of **1**.

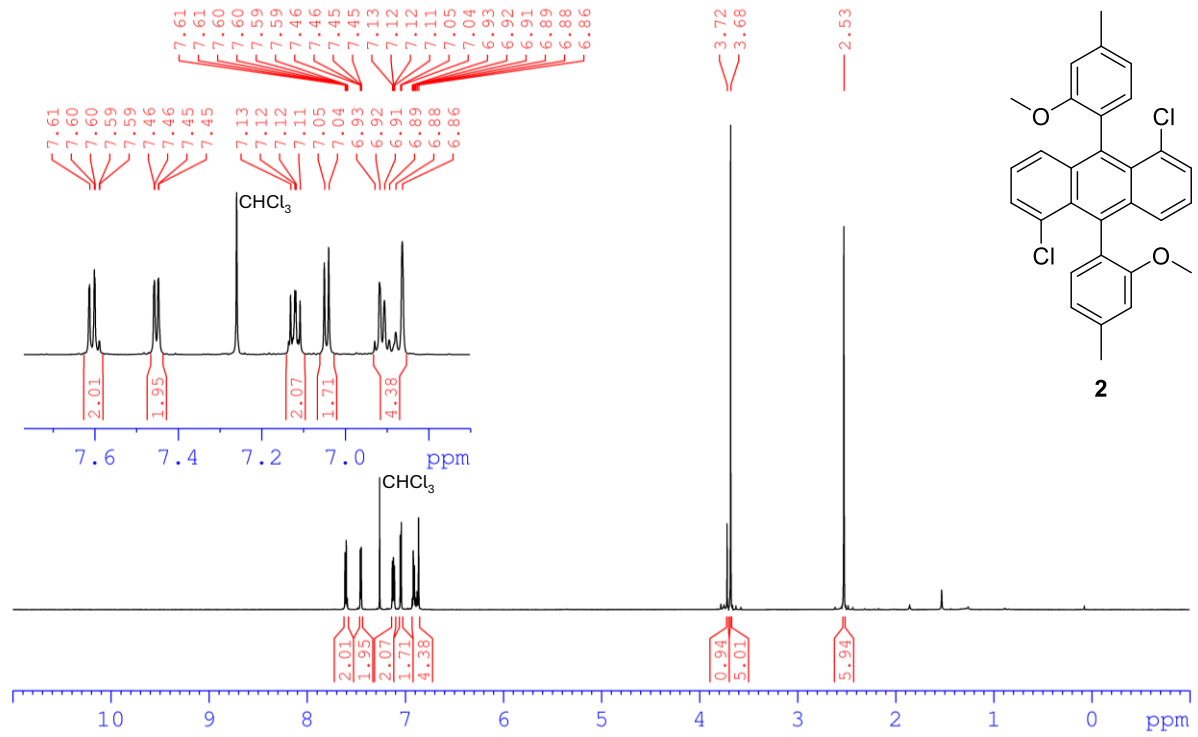

Figure S8. ^{1}H NMR (700 MHz, $CDCl_3$) spectrum of **2**.

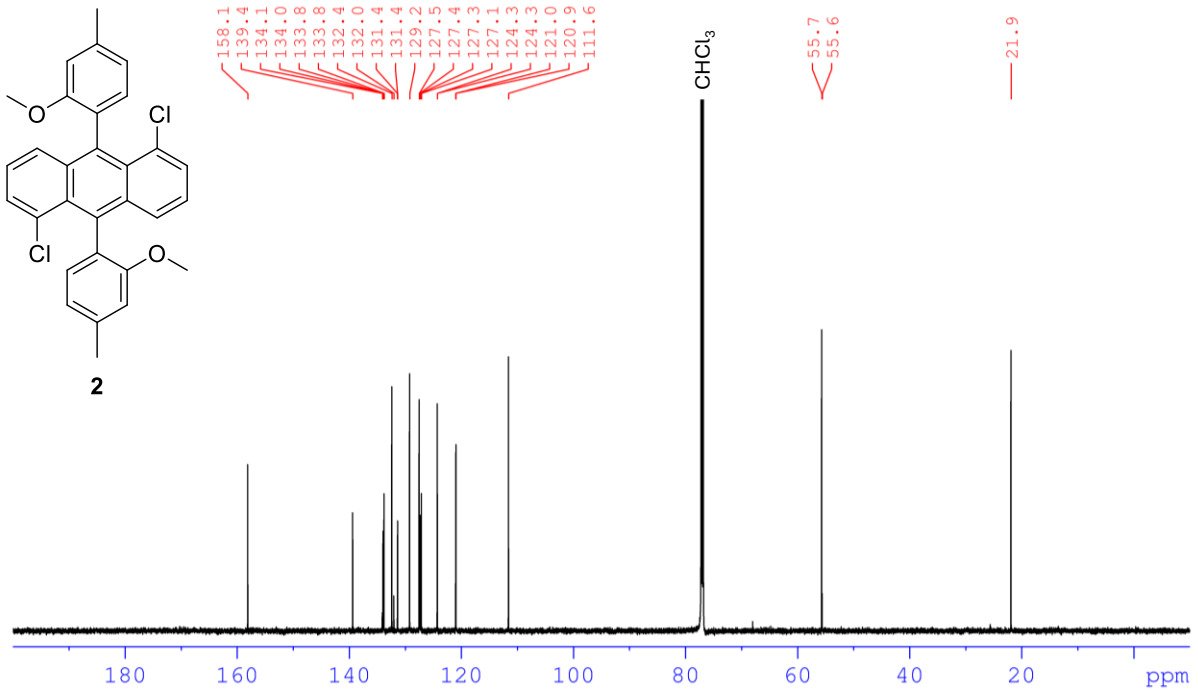

Figure S9. ^{13}C NMR (176 MHz, $CDCl_3$) spectrum of **2**.

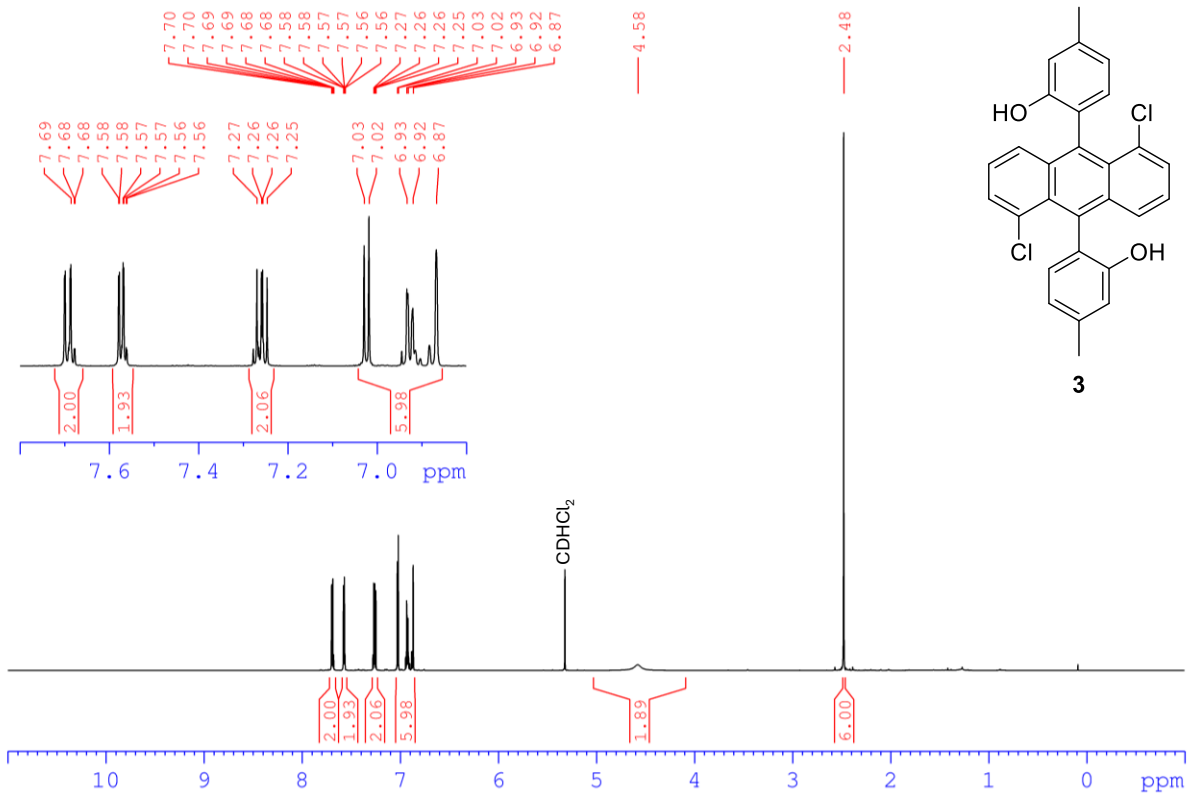

Figure S10. ^{1}H NMR (700 MHz, CD_2Cl_2) spectrum of **3**.

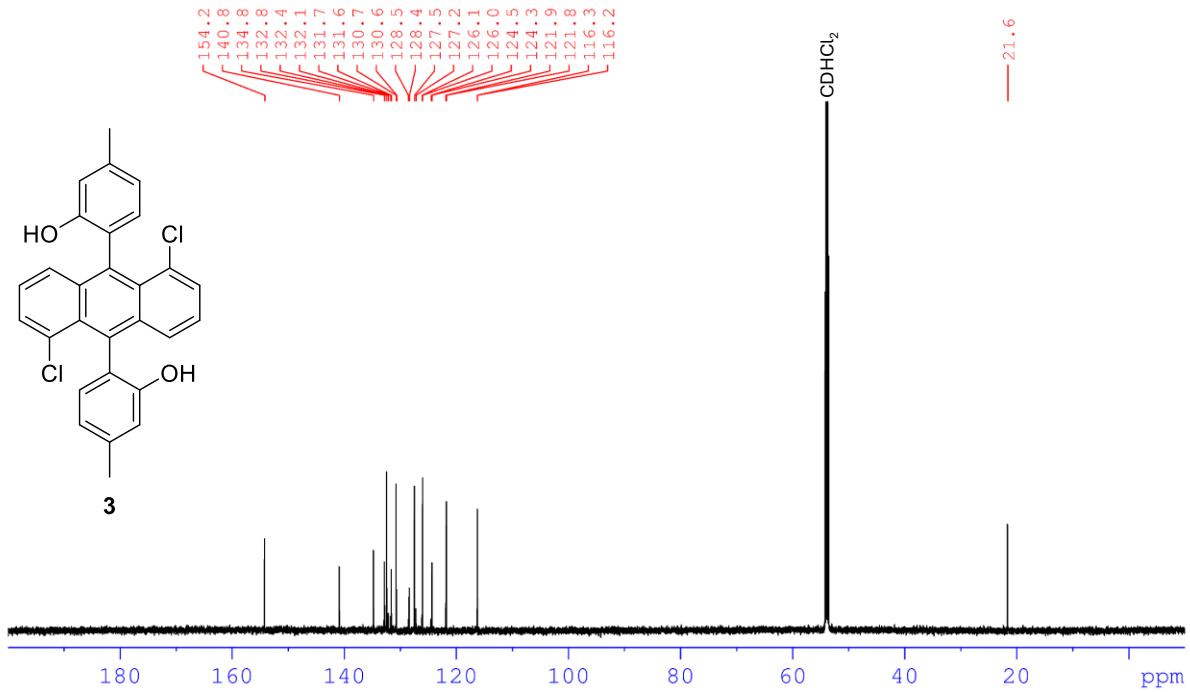

Figure S11. ^{13}C NMR (176 MHz, CD_2Cl_2) spectrum of **3**.

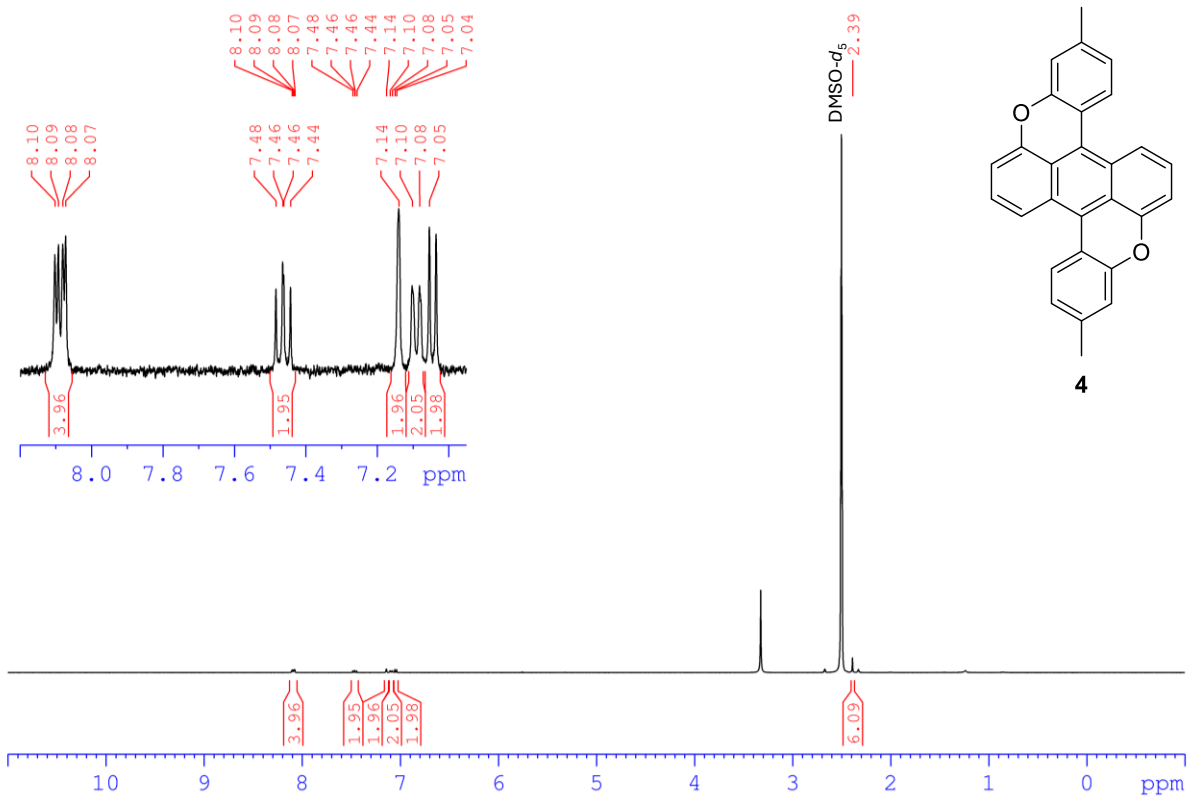

Figure S12. ^{1}H NMR (400 MHz, DMSO-d_6) spectrum of **4**.

5. Mass spectra

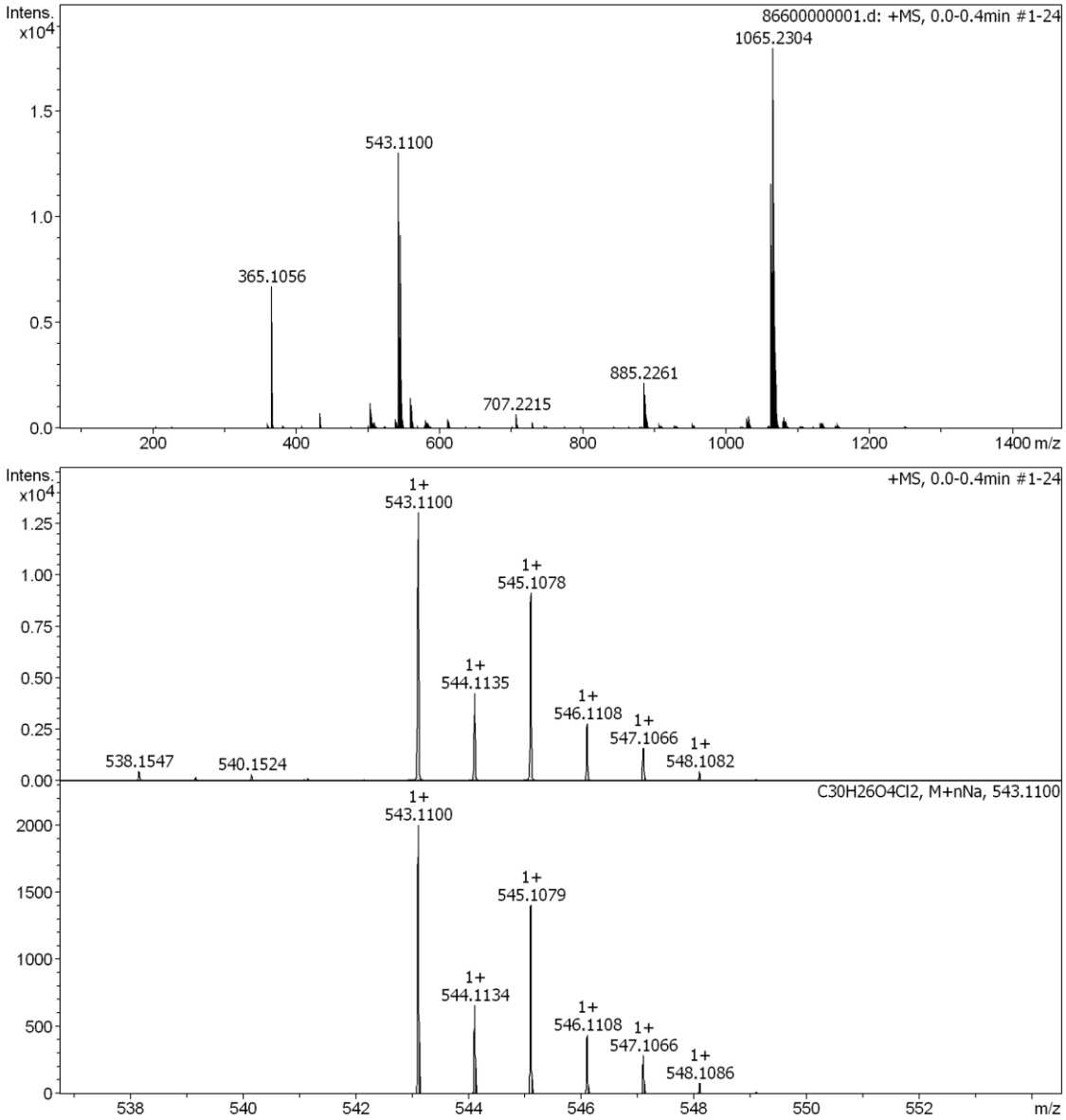

Figure S13. HRMS (ESI^+) spectrum of **1**.

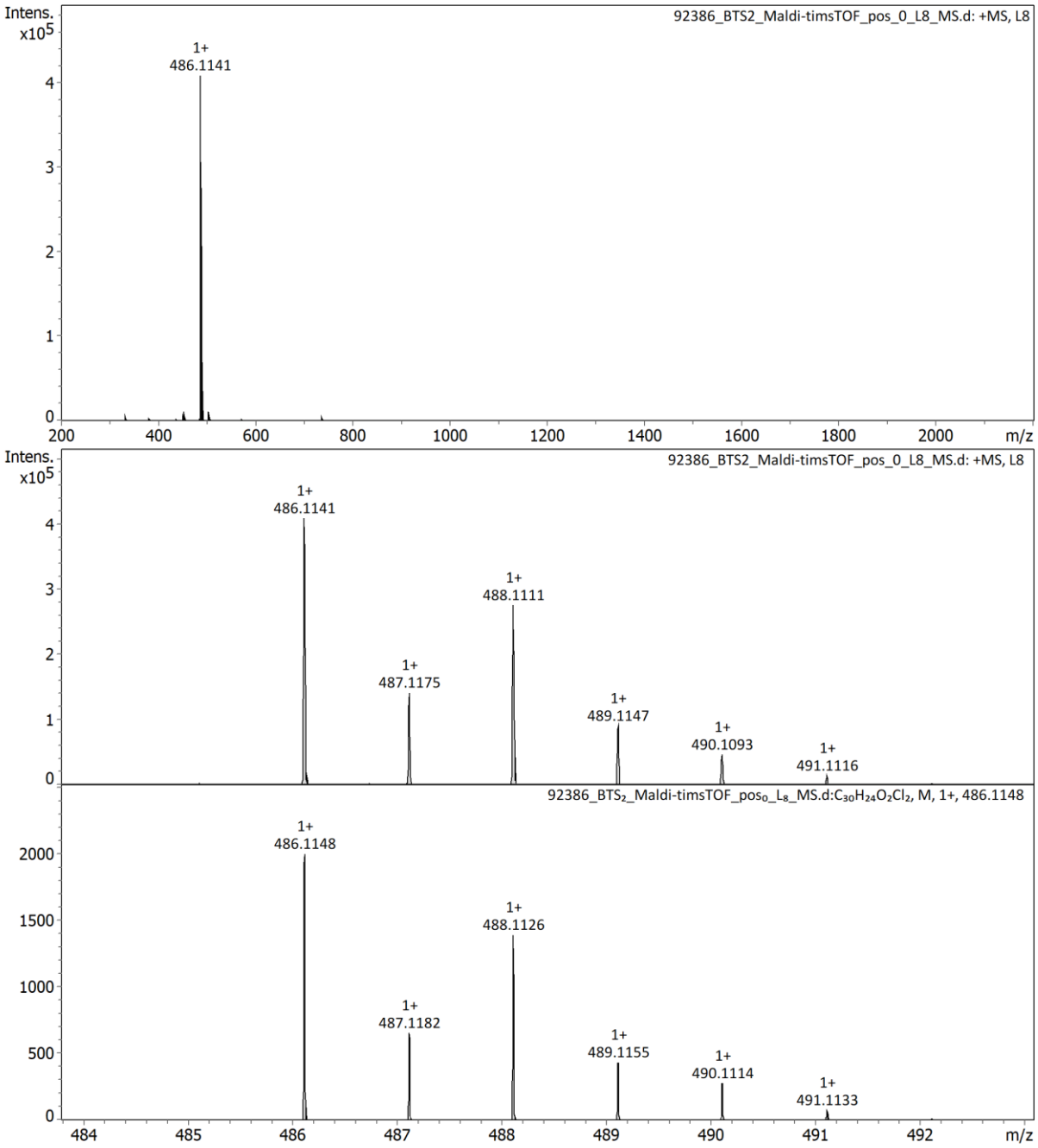

Figure S14. HRMS (MALDI-timsTOF, matrix: DCTB) spectrum of **2**.

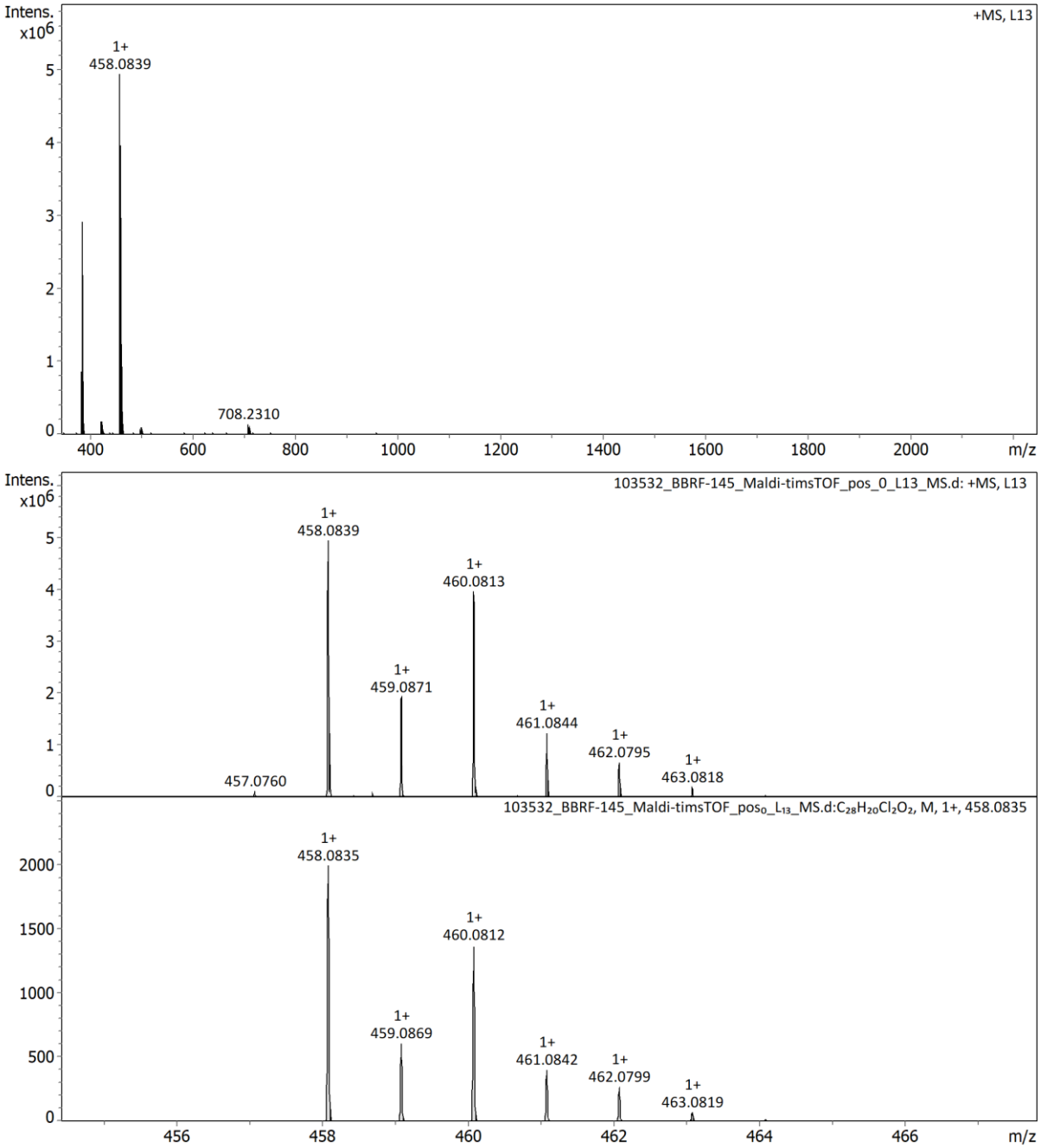

Figure S15. HRMS (MALDI-timsTOF) spectrum of **3**.

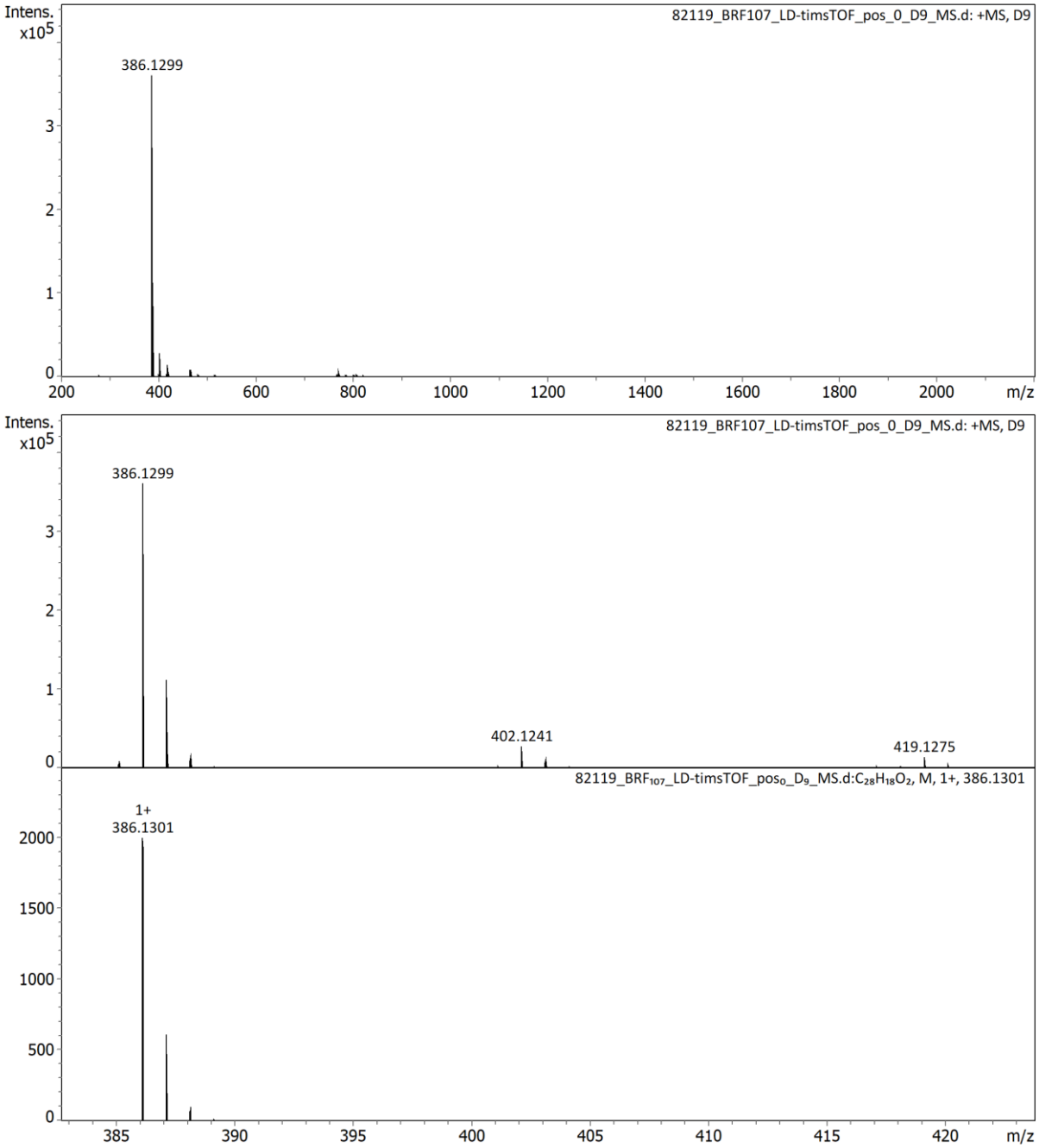

Figure S16. HRMS (LD-timsTOF) spectrum of **4**.

8. Photophysical characterization

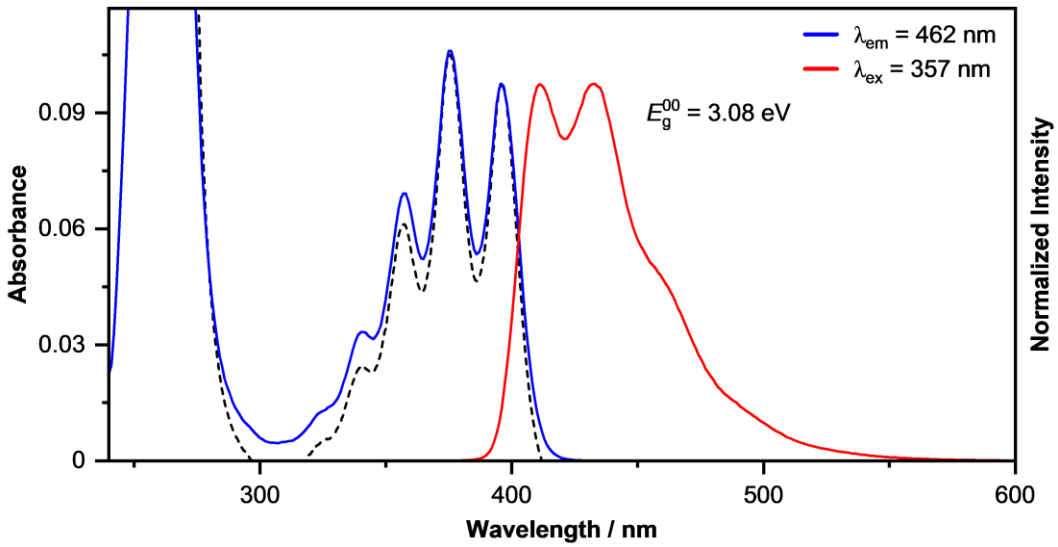

Figure S17. UV-vis absorbance (black, dashed), normalized steady-state excitation (blue), and emission (red) spectra of **DPA** (7.5×10^{-6} M) in $CHCl_3$ at rt.

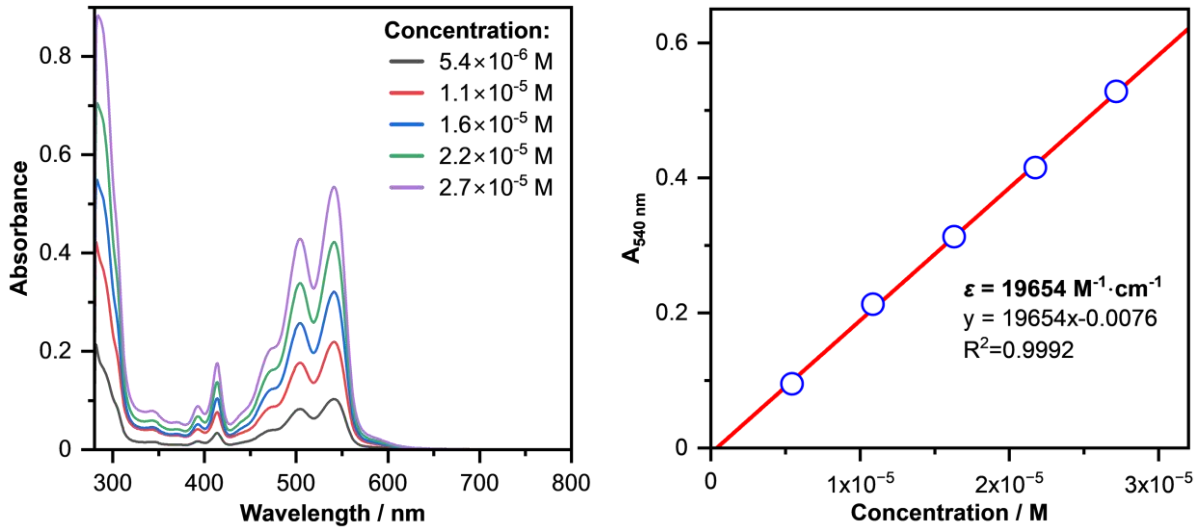

Figure S18. UV-vis absorption spectra (left) of **4** (5.4×10^{-6} M – 2.7×10^{-5} M) in toluene, and determination of the molar attenuation coefficient (right).

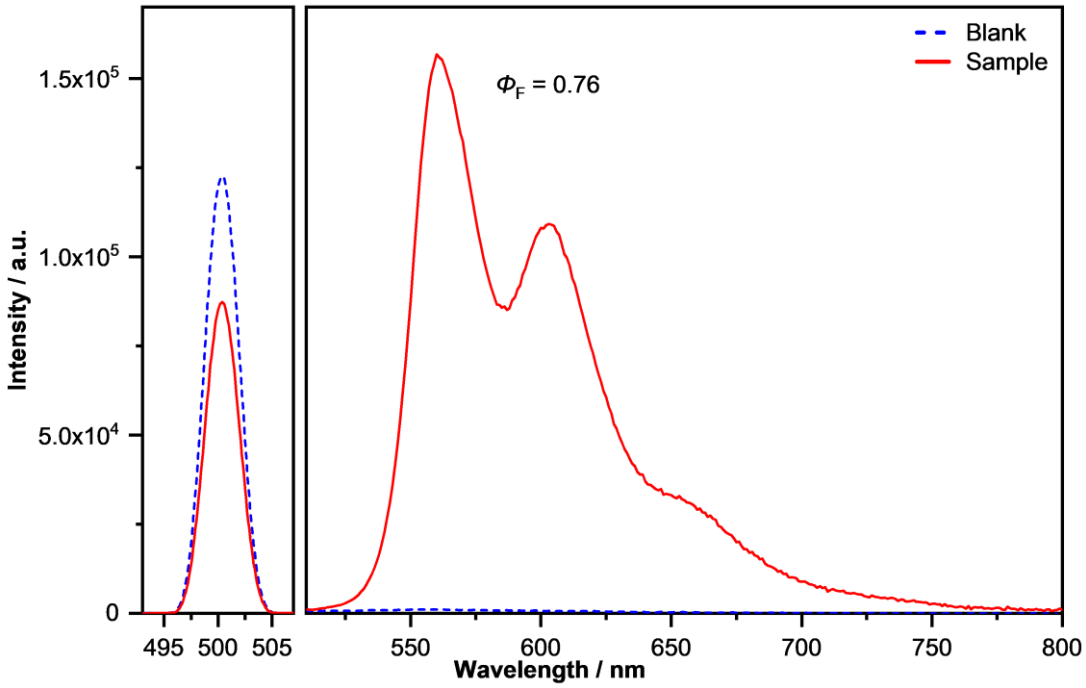

Figure S19. Excitation scatter region (left) and emission spectra (right, λ_{ex} = 500 nm) used to calculate the absolute quantum yield of **4** (6.6×10^{-6} M) in 2-MeTHF.

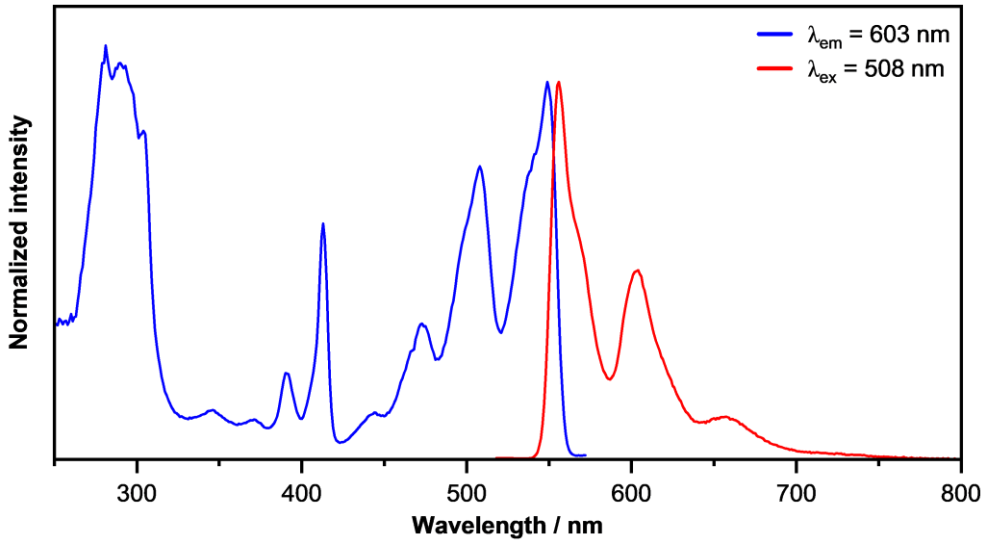

Figure S20. Normalized steady-state excitation (blue) and emission (red) spectra of **4** (6.6×10^{-6} M) in 2-MeTHF at 77K.

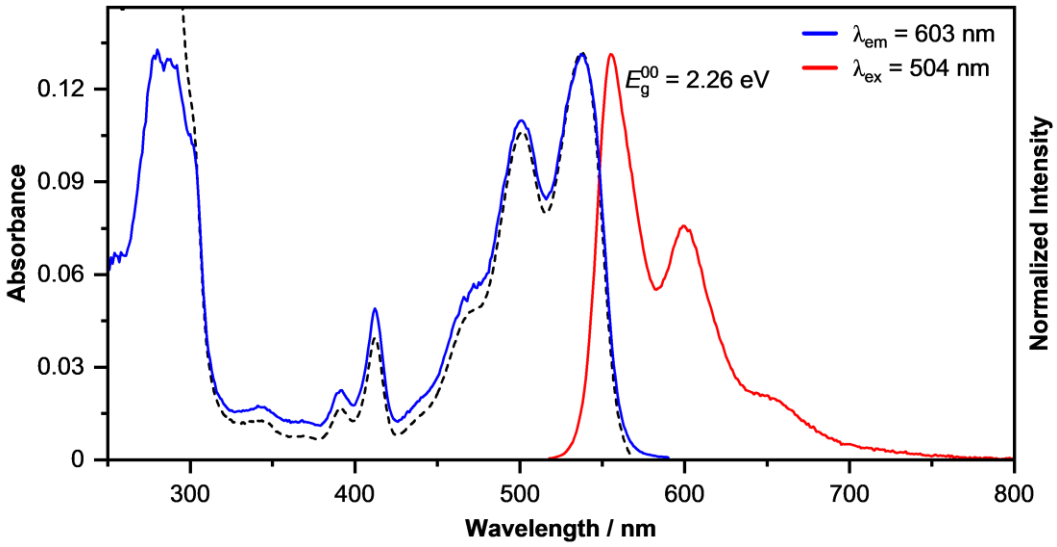

Figure S21. UV-vis absorbance (black, dashed), normalized steady-state excitation (blue), and emission (red) spectra of **4** (6.6×10^{-6} M) in 2-MeTHF at rt.

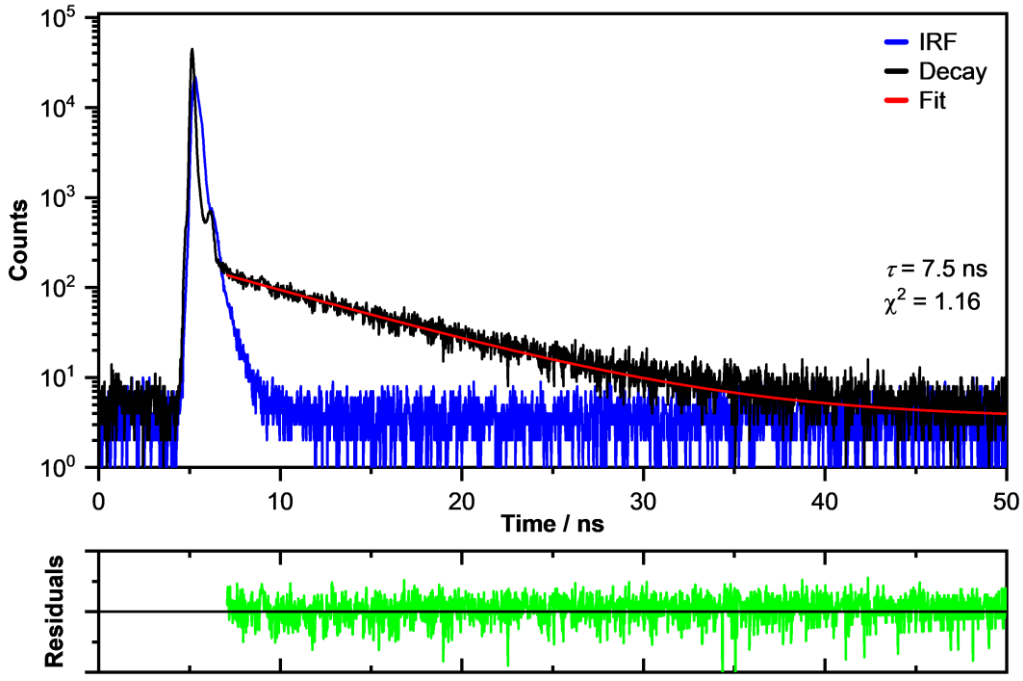

Figure S22. Time-resolved emission decay (λ_{ex}=405.6 nm, λ_{em}=558 nm) of **4** (6.6×10^{-6} M) in 2-MeTHF at rt.

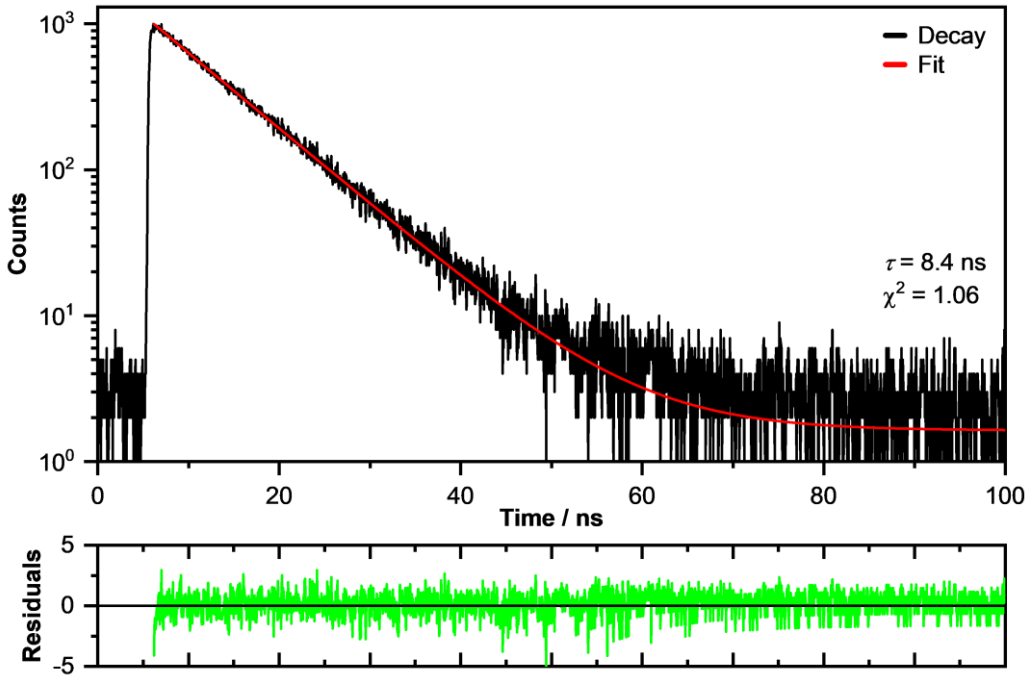

Figure S23. Time-resolved emission decay (λ_{ex}=405.6 nm, λ_{em}=558 nm) of **4** (6.6×10^{-6} M) in 2-MeTHF at 77 K.

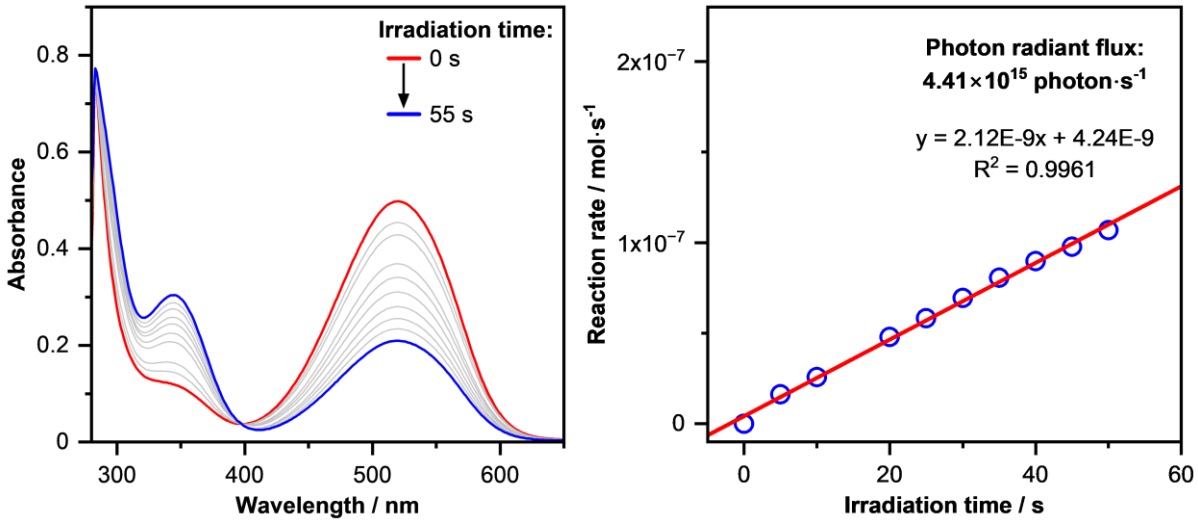

Figure S24. Determination of the photon flux (λ_{ex}=540 nm) of the Xenon irradiation lamp setup using the chemical actinometer Aberchrome 670 (closed form).

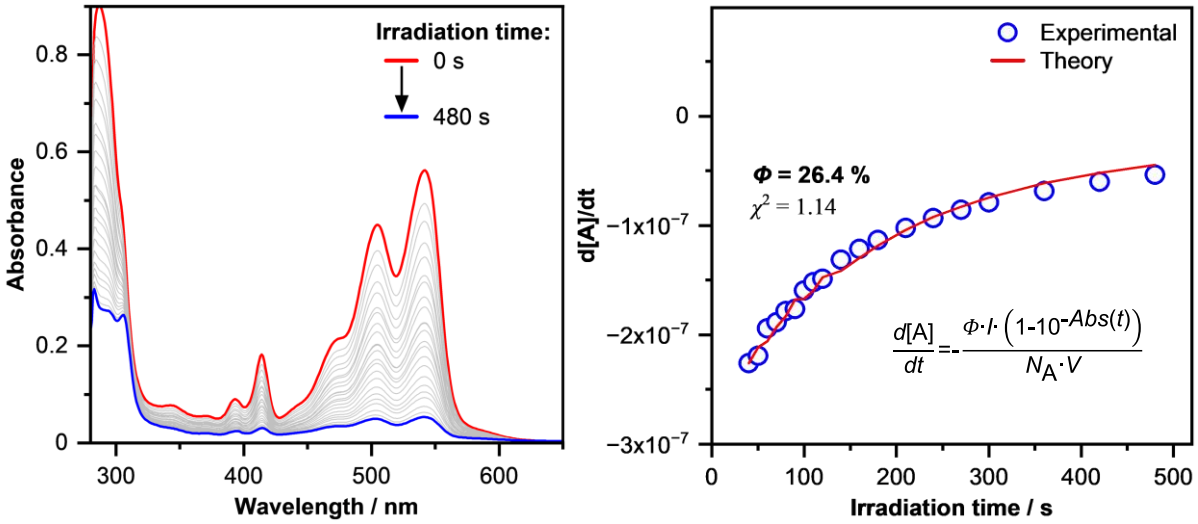

Figure S25. Determination of self-sensitized (λ_{ex} = 540 nm, 2.1 mW/cm^2) photooxidation reaction quantum yield of **4** (2.8×10^{-5}) in toluene at rt.

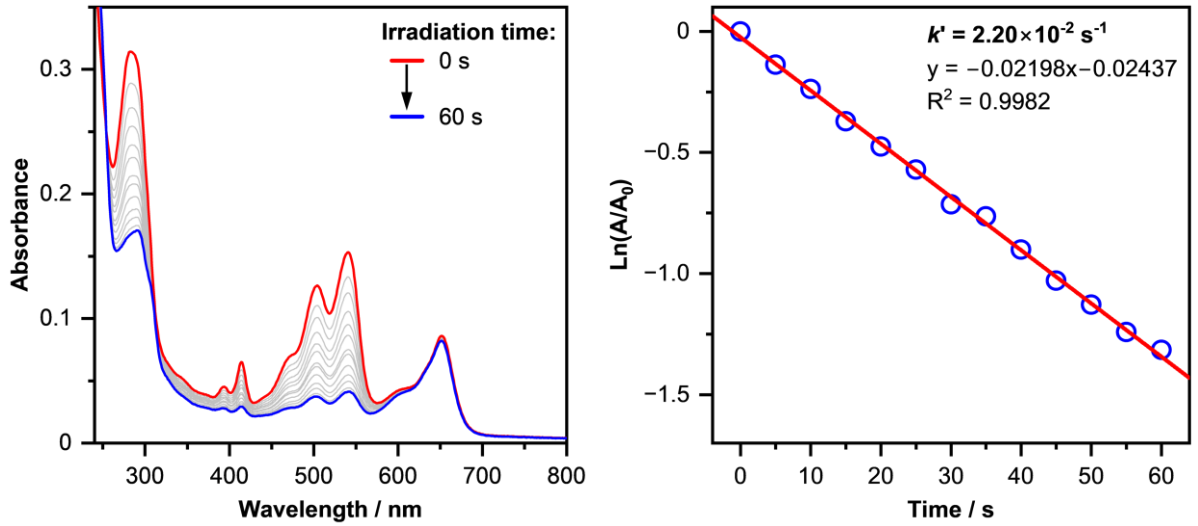

Figure S26. Determination of the photooxygenation pseudo-first-order kinetic constant of **4** (7.8×10^{-6} M) using methylene blue (1.2×10^{-6} M, λ_{ex}=653 nm) as external photosensitizer, in $CHCl_3$.

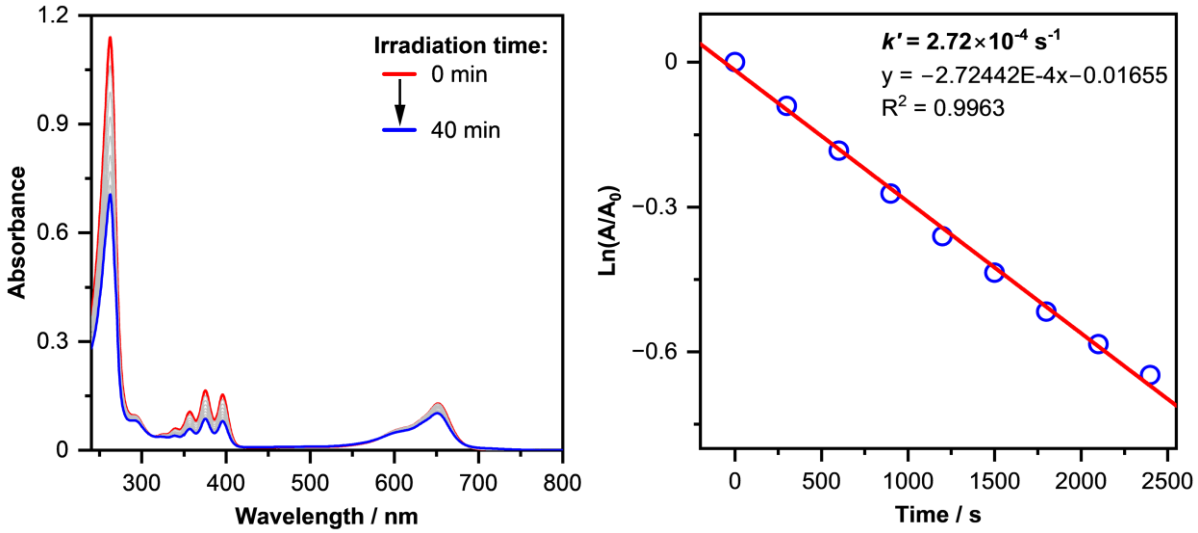

Figure S27. Determination of the photooxygenation pseudo-first-order kinetic constant of **DPA** (1.2×10^{-5} M) using methylene blue (1.2×10^{-6} M, λ_{ex}=653 nm) as external photosensitizer, in $CHCl_3$.

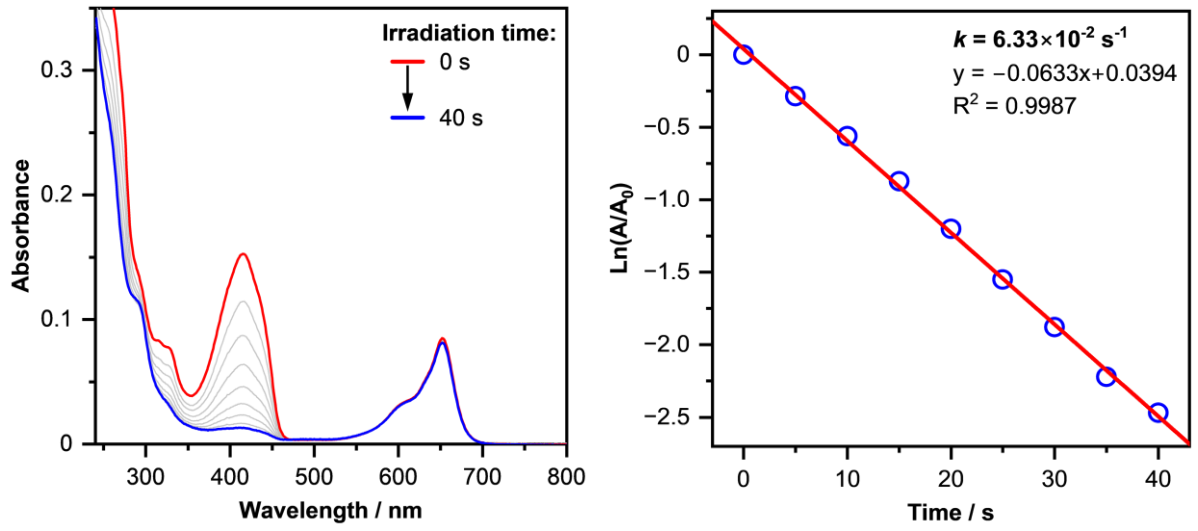

Figure S28. Determination of the photooxygenation pseudo-first-order kinetic constant of **DBPF** (6.6×10^{-6} M) using methylene blue (1.2×10^{-6} M, λ_{ex}=653 nm) as external photosensitizer, in $CHCl_3$.

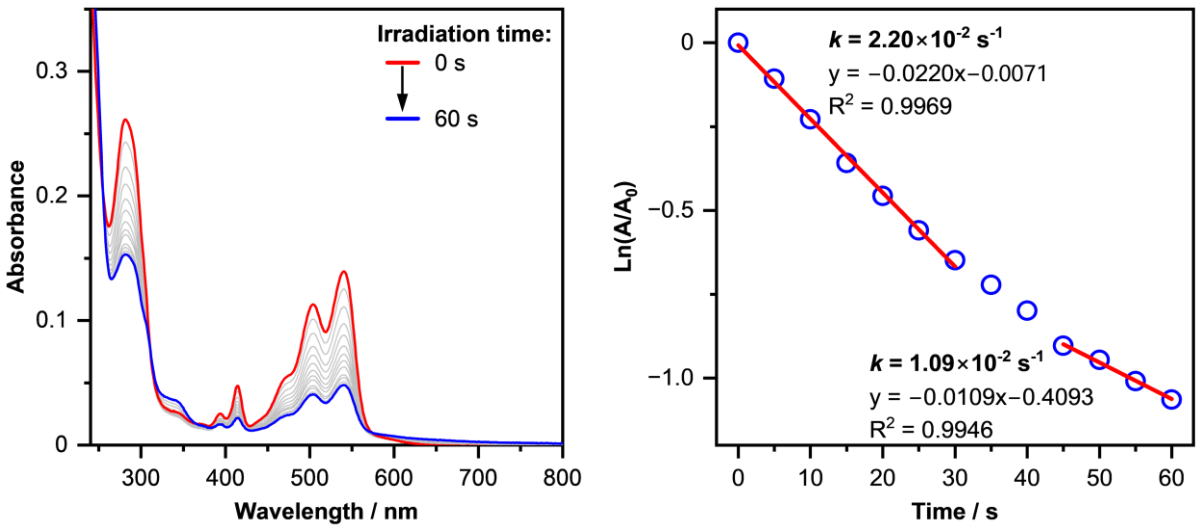

Figure S29. Determination of the self-sensitized photooxygenation pseudo-first-order kinetic constant of **4** (7.8×10^{-6} M, λ_{ex}=540 nm), in $CHCl_3$ at rt.

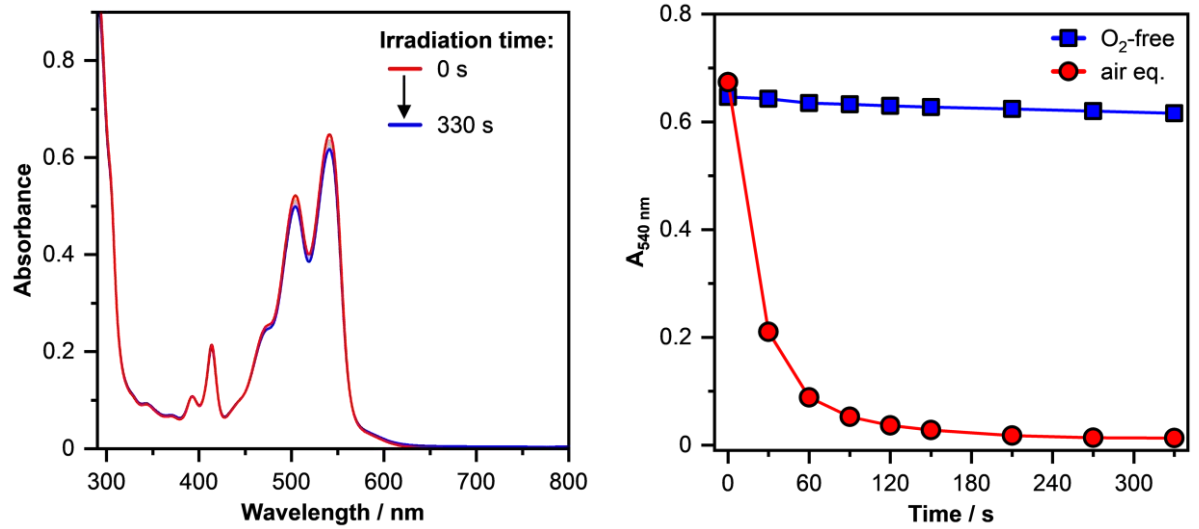

Figure S30. UV-vis recorded as a function of the irradiation time (λ_{ex} = 540 nm, 2.1 mW/cm^2) of a degassed solution of **4** (3.3×10^{-5} M) in toluene (left) and comparison with an air-equilibrated solution (right).

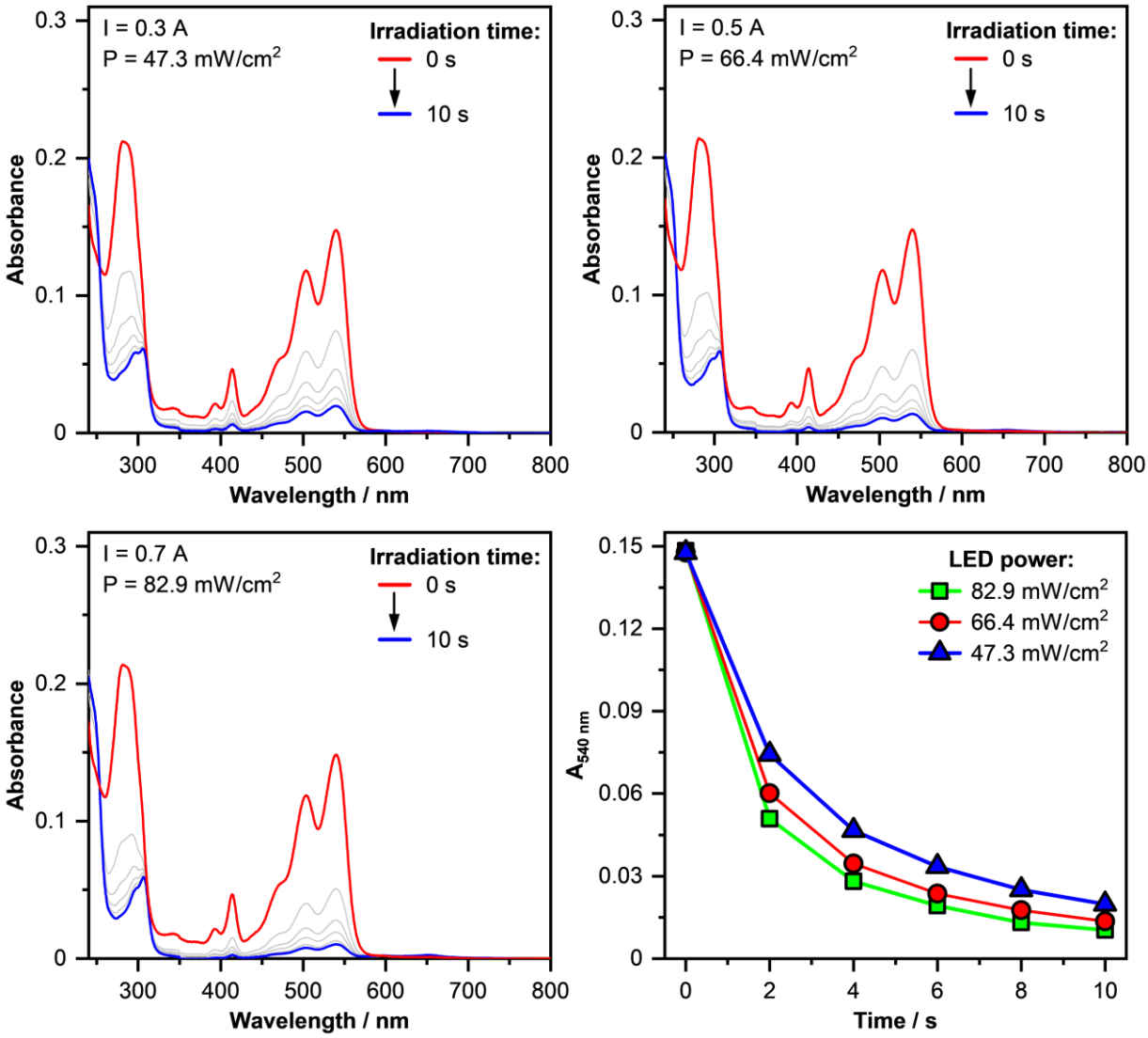

Figure S31. Self-sensitized photooxygenation reaction of **4** (7.5×10^{-6} M) in $CHCl_3$, using different LED (λ_{ex} = 540 nm) irradiation power.

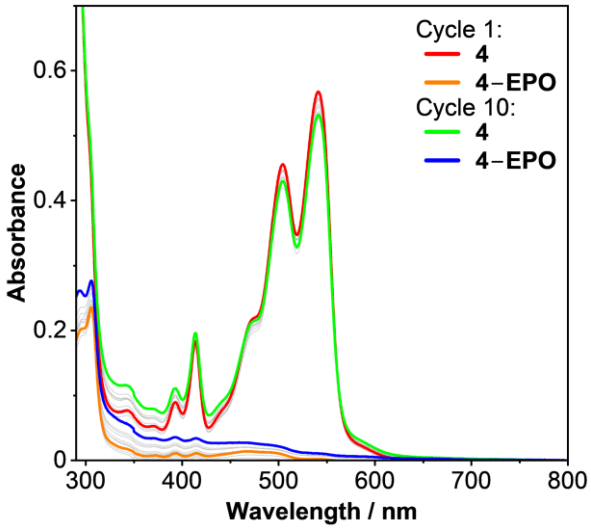

Figure S32. UV-vis absorbance spectra of **4** (2.9×10^{-5} M) over multiple cycles of irradiation (λ_{ex} = 540 nm, 83 mW/cm^2, 30 s) and thermolysis (T = 95 °C, 6 h) in toluene.

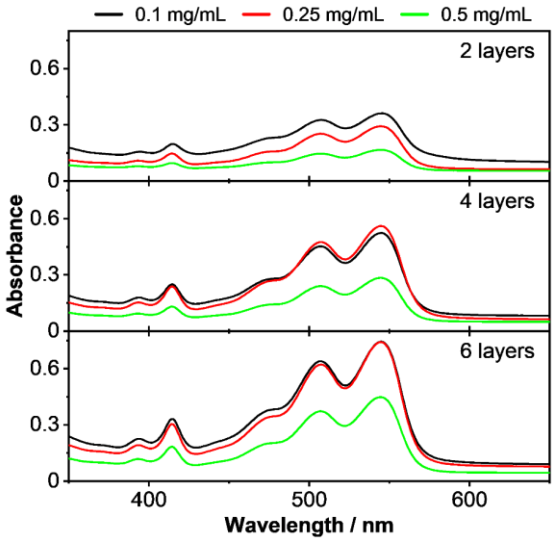

Figure S33. UV–vis absorbance of **4**/DGEBA-DA spray-coated films.

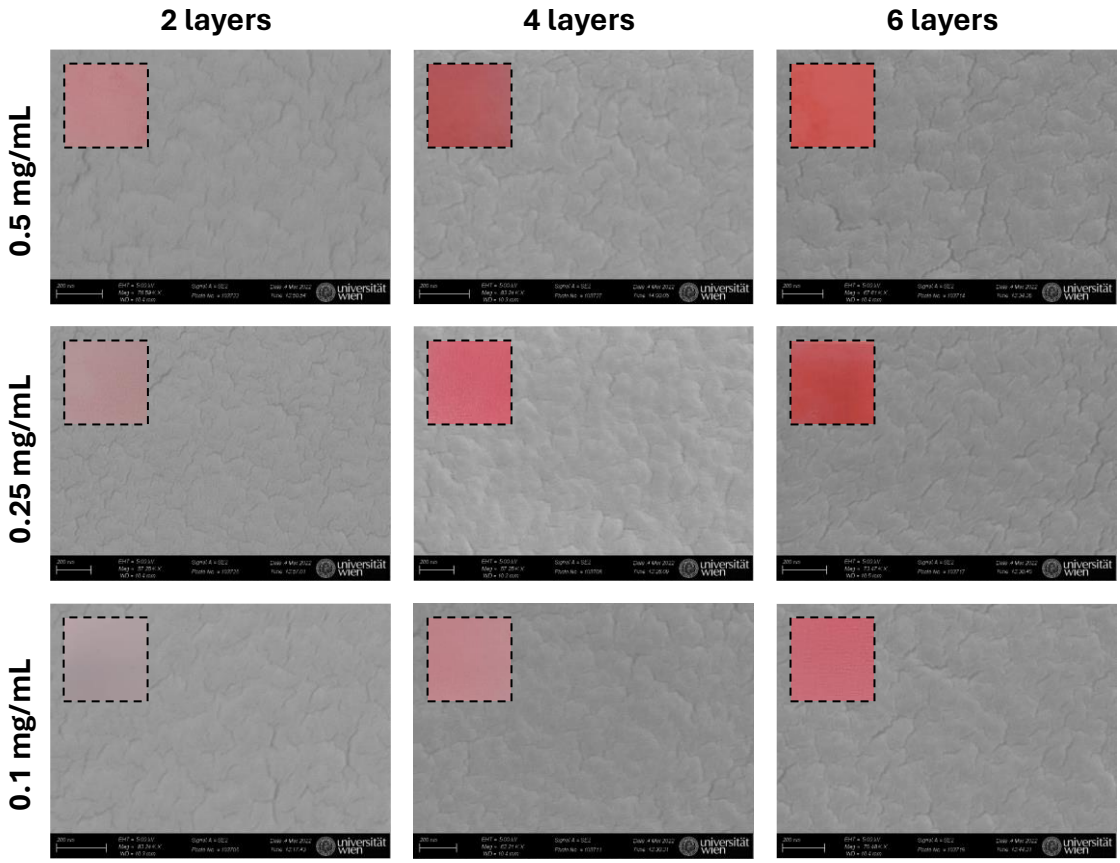

Figure S34. Optical (inset, dashed) and SEM images of **4**/DGEBA-DA spray-coated films.

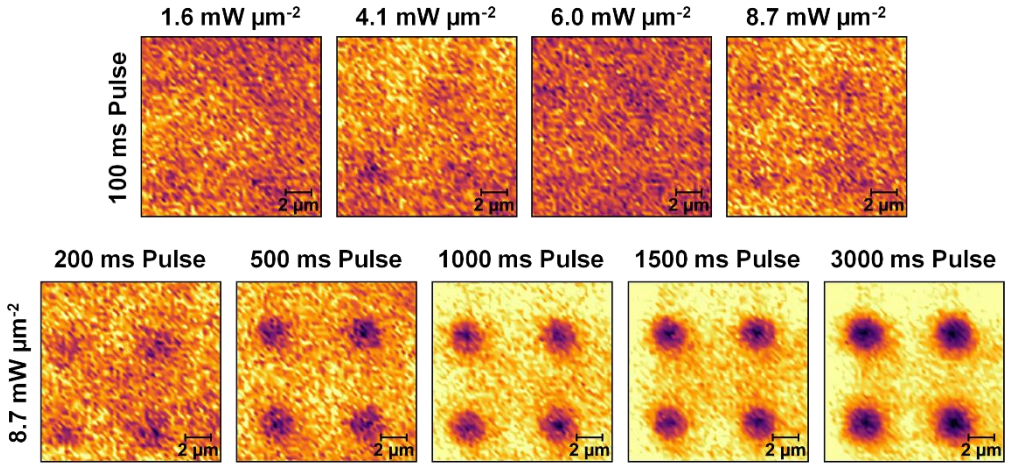

Figure S35. Optimization of the laser pulse duration and power.

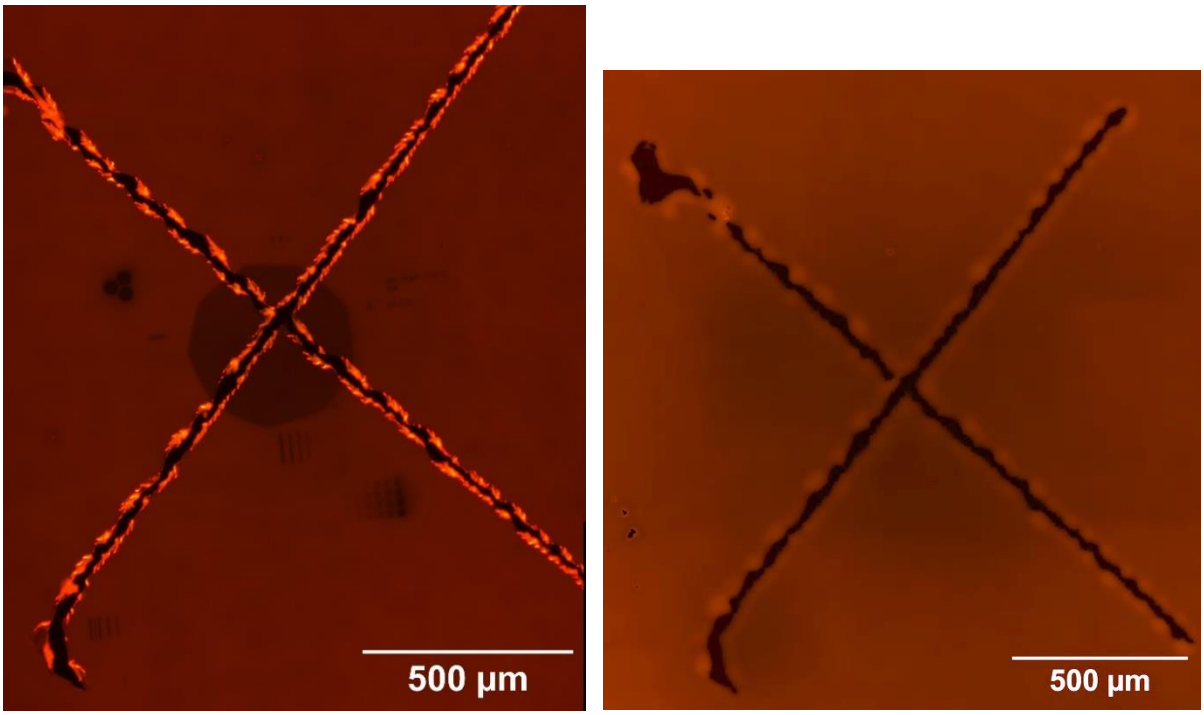

Figure S36. Optical fluorescence microscope pictures after laser writing (left) and after thermal treatment (right, 95°C, 2 h).

10. References

[1] J. Koziskova, F. Hahn, J. Richter, J. Kožíšek, *Acta Chim. Slovaca* **2016**, 9, 136.

[2] G. M. Sheldrick, *Acta Crystallogr A Found Adv* **2015**, 71, 3.

[3] G. Sheldrick, *Acta Crystallogr., Sect. C: Struct. Chem.* **2015**, 71, 3.

[4] C. B. Hübschle, G. M. Sheldrick, B. Dittrich, *J. Appl. Crystallogr.* **2011**, 44, 1281.

[5] O. V. Dolomanov, L. J. Bourhis, R. J. Gildea, J. A. K. Howard, H. Puschmann, *J. Appl. Crystallogr.* **2009**, 42, 339.